

1 Ozone Reactivity Measurement of Biogenic Volatile Organic
2 Compound Emissions

3
4
5 Detlev Helmig^{1,2*}, Alex Guenther³, Jacques Hueber¹, Ryan Daly¹, Wei Wang¹, Jeong-Hoo Park¹,

6
7 Anssi Liikanen⁴, Arnaud P. Praplan⁴

8
9 ¹Institute of Arctic and Alpine Research, University of Colorado, Boulder, CO 80309, USA

10 ²~~now~~^{now} at: Boulder Atmosphere Innovation Research LLC, Boulder, CO 80305, USA

11 ³~~University~~^{University} of California Irvine, CA, USA

12 ⁴Atmospheric Research Composition, Finnish Meteorological Institute, 00101 Helsinki, Finland

13 *corresponding author: dh.bouldair@gmail.com

14
15 *Manuscript submitted to*

16 *Revised manuscript for publication in*

17
18 Atmospheric Measurement Techniques

19
20 ~~October 25, 2021~~

21 March 31, 2022

22
23 **Abstract**

24
25 Previous research on atmospheric chemistry in the forest environment has shown that the total
26 reactivity by biogenic volatile organic compound (BVOC) emission is not well considered in forest
27 chemistry models. One possible explanation for this discrepancy is the unawareness and neglect of
28 reactive biogenic emission that have eluded common monitoring methods. This question motivated
29 the development of a total ozone reactivity monitor (TORM) for the direct determination of the
30 reactivity of foliage emissions. Emissions samples drawn from a vegetation branch enclosure
31 experiment are mixed with a known and controlled amount of ozone (~~e.g.~~ resulting in e.g. 100 ppb
32 of ozone) and directed through a temperature-controlled glass flow reactor to allow reactive biogenic
33 emissions to react with ozone during the approximately 2-minute residence time in the reactor. The
34 ozone reactivity is determined from the difference in the ozone mole fraction before and after the
35 reaction vessel. An inherent challenge of the experiment is the influence of changing water vapor in
36 the sample air on the ozone signal. A commercial UV absorption ozone monitor was modified to
37 directly determine the ozone differential with one instrument and sample air was drawn through
38 Nafion dryer membrane tubing. These two modifications significantly reduced interferences from
39 water vapor and errors associated with the determination of the reacted ozone ~~compared to~~
40 determining as the difference from two individual measurements ~~and errors from interferences~~
41 from water vapor, resulting in a much improved and sensitive determination of the ozone reactivity.
42 This paper provides a detailed description of the measurement design, the instrument apparatus,
43 and its characterization. Examples and results from field deployments demonstrate the applicability
44 and usefulness of the TORM.

46
47
48
49
50
51
52
53
54
55
56
57
58
59
60
61
62
63
64
65
66
67
68
69
70
71
72
73
74
75
76
77
78
79
80
81
82
83
84
85
86
87
88
89
90
91

1. Introduction

Recent field research on the atmospheric chemistry in forest environments has yielded a series of results that cannot be explained with our current comprehension of biogenic emissions, deposition processes, and chemical reactions. These findings date back to the pivotal paper by ~~Di Carlo et al. [2004]~~ Di Carlo et al. [2004] that stimulated new interest and research into the question of unaccounted for biogenic volatile organic compound (BVOC) emissions. These researchers compared the directly measured hydroxyl radical (OH) reactivity in ambient air at the University of Michigan Biological Station (UMBS) PROPHET forest research site with the OH reactivity calculated from a comprehensive set of measured atmospheric gas phase species. The important conclusion of this study was that identified compounds could only account for about 2/3 of the directly measured OH reactivity. Interestingly, the difference between the two measurements, often called “missing OH reactivity” showed temperature dependence very similar to that found for monoterpene (MT) compounds. This similarity led the authors to hypothesize that the missing OH reactivity is due to non-identified BVOC emissions emitted from tree foliage at this site.

While these findings were surprising at the time of publication, several other subsequent studies have come to similar conclusions. OH reactivity measurements in ambient air have consistently shown higher OH reactivity values than what can be accounted for by quantified chemical species, and notably, the review of available measurements shows a tendency towards a higher discrepancy at sites that are subjected to a relatively high influence from BVOC emissions ~~[Lou et al., 2010].~~ [Lou et al., 2010].

The other line of research that has pointed towards the current underestimation of BVOC emissions relies on ozone flux observation over forest canopies. ~~Kurpius and Goldstein [2003]~~ Kurpius and Goldstein [2003] segregated ozone deposition fluxes over a ponderosa pine plantation into stomatal uptake, non-stomatal surface deposition, and gas phase chemistry contributions. They found that during summer, the ozone flux was dominated by gas-phase chemistry, and that the ozone loss showed an exponential increase with temperature, with similar behavior as BVOC emissions. However, identified BVOCs could only account for a small fraction of this reactivity. Consequently, these researchers postulated that there is a “large unrecognized source of reactive compounds in forested environments”. ~~A follow-up study [Goldstein et al., 2004].~~ A follow-up study [Goldstein et al., 2004]. based on measurements during a forest thinning experiment, went even further and claimed that “unmeasured BVOC emissions are approximately 10 times the measured monoterpene flux”. These hypotheses have been supported by findings from ~~other subsequent studies [Altimir et al., 2004; Holzinger et al., 2005; Altimir et al., 2006; Hogg et al., 2007; Fares et al., 2010a; Fares et al., 2010b; Fares et al., 2010c; Wolfe et al., 2011].~~ a series of other subsequent studies [Altimir et al., 2004; Holzinger et al., 2005; Altimir et al., 2006; Hogg et al., 2007; Fares et al., 2010a; Fares et al., 2010b; Fares et al., 2010c; Wolfe et al., 2011].

There has been considerable progress in identifying and characterizing hitherto unrecognized BVOC emissions. The most significant ones are light-dependent MT emissions ~~[Ortega et al., 2007; McKinney et al., 2011]~~ [Ortega et al., 2007; McKinney et al., 2011] and sesquiterpenes (SQT) ~~[Duhl et al., 2008].~~ Furthermore, it has been ~~recognized that methyl chavicol can be an important emission [Bouvier-Brown et al., 2009a; Bouvier-Brown et al., 2009b; Misztal et al., 2010].~~ [Ortega et al., 2007; McKinney et al., 2011] and

92 sesquiterpenes (SQT) [Duhl et al., 2008]. Furthermore, it has been recognized that methyl chavicol
93 can be strongly emitted [Bouvier-Brown et al., 2009a; Bouvier-Brown et al., 2009b; Misztal et al.,
94 2010]. However, inclusion of these emissions only contributes a minor fraction to closing the gap
95 between identified and inferred BVOC emissions. ~~In a study at the PROPHET site, using the~~
96 comparative reactivity method, Kim et al. [2011] concentrations. In a study at the PROPHET site,
97 using the comparative reactivity method, Kim et al. [2011] determined directly the OH reactivity in
98 emission samples drawn from branch enclosures. OH reactivity was also calculated based on BVOC
99 emissions identified by Proton Transfer Reaction Mass Spectrometry (PTR-MS) and Gas
100 Chromatography Mass Spectrometry (GC-MS). A red oak, white pine, beech, and maple tree were
101 investigated. Their results indicated a high range of total OH reactivity from the emissions of these
102 species, with red oak emissions showing the highest OH reactivity overall. Identified isoprene and
103 MT emissions could explain the directly measured OH reactivity from red oak, white pine, and beech.
104 However, isoprene and monoterpene emissions from red maple could only explain a fraction of the
105 measured OH reactivity. The OH reactivity from maple was dominated by emission of the SQT α -
106 farnesene, which is a compound that would not have been identified in earlier studies of ambient
107 BVOC at this site. These findings show that the chemical reactivity in emissions from different tree
108 species can vary substantially in their overall magnitude and attribution to the emitted BVOC species.
109 This indicates that there is the potential that ecosystems with different plant species composition
110 could have substantial unaccounted for emissions that contribute to OH reactivity. This suggests that
111 there must be BVOC compounds or compound classes emitted from foliage that current
112 measurements do not capture, which is not unexpected given the major analytical challenges
113 associated with analysis of some organic compounds.

114
115 In this work, we are describing a monitoring approach that addresses this dilemma by constraining
116 the total ozone reactivity of BVOCs emissions with a direct measurement. These observations can
117 be contrasted with the reactivity that is calculated from the sum of the reactivities of individual BVOCs
118 and their OH reaction rates to assess the fraction of the identified and missing compounds that
119 contribute to the total reactivity. The instrument relies on a flow reactor. Sample air containing BVOCs
120 is mixed with a small flow containing a high mole fraction of ozone. The loss of ozone is monitored
121 with a differential ozone measurement. Our Total Ozone Reactivity Monitor (TORM) that was
122 previously presented in ~~[Helmig et al., 2010; Park et al., 2013]~~[Helmig et al., 2010; Park et al., 2013]
123 has since undergone further testing and development. The calculation of ozone reactivity is
124 explained in Supplement A, and the modelled decay of a few typically measured BVOC and ozone
125 in the reactor is available in Supplement B.

126
127 Two other instruments relying on different types of reactor and detection methodology have been
128 reported since ~~[Matsumoto, 2014; Sommariva et al., 2020].~~[Matsumoto, 2014; Sommariva et al.,
129 2020]. These previous publications have also provided the principle and reaction kinetics
130 consideration for this measurement. A linear double-tube Pyrex glass tube flow reactor with ozone
131 detection up- and downstream of the reactor by two modified commercial (ECO PHYSICS, CLD770)
132 chemiluminescence detectors (CLD) was used in the work by ~~Matsumoto [2014].~~Matsumoto [2014].
133 The ozone reactivity was determined from the difference of the two analyzers' signal. A 1 m long, 2.4
134 L volume-PTFE linear reactor ~~was used by Sommariva et al. [2020].~~was used by Sommariva et al.
135 [2020]. These authors used two commercial Thermo Scientific Model 49i UV absorption monitors for
136 the ozone determination, with the ozone reactivity again determined from the difference of the two
137 monitor signals.

139 We particularly emphasize the necessity of properly characterizing the interference from water vapor
140 on the ozone determination, and the advantage of the measurement of the amount of reacted ozone
141 through a differential ozone determination with a single monitor. Thirdly, assembly of readily available
142 instrument components facilitate a relatively easy, low expense instrument assembly.

143
144 Rigid chambers or flexible bag enclosures are the common approaches for studying biogenic
145 emissions by dynamic or static vegetation enclosures ~~[Ortega and Helmig, 2008; Ortega et al.,~~
146 ~~2008].~~[Ortega and Helmig, 2008; Ortega et al., 2008]. Enclosure experiments allow the selective
147 identification of emissions from individual plant species. Depending on the operational parameters,
148 emissions can build up to many times, even order of magnitudes, higher levels than in ambient air.
149 Higher temperatures (than in ambient air) are often encountered inside enclosures from the
150 greenhouse warming effect, which enhances emissions and facilitates higher sensitivity of emissions
151 determination. An inherent disadvantage and analytical challenge, however, is the evaporative water
152 flux from the transpiring enclosed foliage. Under the most extreme, and not too uncommon
153 conditions, water vapor saturation can be achieved inside the chamber, causing liquid water
154 condensation on the chamber inside walls and within sampling tubing. The water flux is sensitive to
155 the stomatal conductance, responding to conditions of light and temperature. In an ambient setting,
156 these often change dynamically, causing similarly fast changes in water vapor concentration inside
157 the enclosure and sample air. At ~~30°C~~30°C and water saturation, the water vapor mole fraction is
158 approximately 4.2%. A mere 10-% fluctuation equates to 4.2 parts per thousand, ~~(%)~~, or 4,200,000
159 ppb of a water vapor change. The signals that have been achieved in ozone reactivity monitoring
160 instruments system are usually in the single ppb range ~~for $\Delta[O_3]$~~ . Consequently, for the ozone
161 monitoring to be selective, the ozone detection needs to be insensitive to water vapor changes that
162 can be on the order of 10^6 - 10^7 times larger in mole fraction than the ozone signal. This is an
163 enormous challenge for this measurement, as both the ozone CLD and UV absorption
164 measurements are sensitive to water vapor.

165
166 Interference with an instrument signal response in the range of tens to hundreds of ppb has been
167 reported for different types of UV absorption monitors from rapid changes in water vapor ~~[Wilson~~
168 ~~and Birks, 2006; Spicer et al., 2010].~~[Wilson and Birks, 2006; Spicer et al., 2010]. This interference
169 was traced to humidity effects on the transmission of light, i.e. reflectivity of light on the cell walls,
170 through the optical cell ~~[Wilson and Birks, 2006].~~[Wilson and Birks, 2006]. The study identified that
171 the instrument's ozone scrubber amplified this effect, acting as a water reservoir adding or removing
172 water to the air flow depending on the sample air moisture content. A 10 % change in the recorded
173 ozone was observed from a 30 to 80-% RH increase for a UV absorption monitor ~~[Kim et al., 2019;~~
174 ~~Kim et al., 2020].~~in other studies [Kim et al., 2019; Kim et al., 2020]. Inserting a Nafion dryer into the
175 sampling path can reduce the water interference, in the best scenario to within equal or better than
176 ± 2 ppb ~~[Wilson and Birks, 2006; Spicer et al., 2010; Kim et al., 2020].~~ ~~Sommariva et al. [2020]~~[Wilson
177 and Birks, 2006; Spicer et al., 2010; Kim et al., 2020]. ~~Sommariva et al. [2020]~~ found that the ozone
178 wall losses were dependent on the relative humidity in their PTFE flow reactor.

179
180 While CLD analyzers for ozone determination are more expensive to acquire and operate, they are
181 popular for fast ozone measurements such as for aircraft ~~[Ridley et al., 1992]~~[Ridley et al., 1992] and
182 eddy covariance flux measurements ~~[Lenschow et al., 1981, 1982].~~[Lenschow et al., 1981, 1982].
183 Similarly to UV monitors, CLD instruments suffer from an interference by water vapor, which in this
184 case is caused by the quenching of the chemiluminescence signal in the reaction chamber

185 ~~[Matthews et al., 1977; Boylan et al., 2014].~~[Matthews et al., 1977; Boylan et al., 2014]. A correction
186 factor of $4\text{-}5 \times 10^{-3}$ has been proposed, to be multiplied by the water vapor mole fraction in nmol mol^{-1}
187 ~~[Boylan et al., 2014].~~[Boylan et al., 2014]. Under moist ambient air conditions, this correction can
188 account for up ~~to 15 to 15%~~ of the ozone signal. Consequently, following the enclosure system water
189 vapor estimates above, CLD in an ozone reactivity system may be susceptible to a several percent
190 interference from changing water vapor, which is on the same order of magnitude as the observed
191 ozone reactivity observed in the flow chamber system.

192 ~~Both, Matsumoto [2014] and Sommariva et al. [2020]~~

193 Both, Matsumoto [2014] and Sommariva et al. [2020] used two ozone monitors for determination of
194 the ozone upstream and downstream of the reactor, with the reacted ozone then determined as the
195 difference of the recordings from both instruments. One objective of this configuration in the
196 ~~Matsumoto [2014]~~Matsumoto [2014] work was to achieve a reduction of the quenching interference,
197 based on the assumption that both monitors would have similar responses to the water interferences,
198 with these errors then mostly cancelling out in the differential ozone reactivity signal calculation.
199 From a measurement and signal perspective, this is a rather disadvantageous measurement
200 approach for several reasons: (1) the two monitors need to be carefully synced/calibrated against
201 each other to make sure the instrument offset is characterized and corrected for so that their readings
202 are consistent; (2) drifts of any of the two monitors, or of both, will directly transfer to a measurement
203 error in ~~the ozone reactivity signal;~~ $\Delta[\text{O}_3]$; and (3), statistically, the calculation of the ozone reactivity
204 will be subject to a relatively large error, as the ~~ozone reactivity~~differential signal is a relatively small
205 value resulting from the difference between two larger numbers. Any absolute errors in the directly
206 measured values will therefore transfer into a relatively large error of the smaller differential. For
207 these reasons, it would be preferable to measure the ozone differential through a direct
208 measurement with one monitor. Furthermore, a one monitor measurement would be advantageous
209 in terms of instrument maintenance and cost.

210

211 Our experiment presented here overcomes this predicament by modifying a commercial UV
212 absorption ozone monitor for the direct measurement of the ozone differential. Further, sample drying
213 was implemented to reduce the aforementioned interference from fluctuations in the sample water
214 vapor mole fraction. The experiments described here were conducted ~~successively on two similar~~
215 ~~systems at the University of Colorado, Boulder, and the Finnish Meteorological Institute (FMI) in~~
216 ~~Helsinki, Finland.~~ on two similar systems. The first instrument was developed at the University of
217 Colorado, Boulder (CU). Colleagues from the Finnish Meteorological Institute (FMI) in Helsinki visited
218 CU for collaborative research on the experiment and then constructed a similar instrument to be
219 used for their research at FMI. Both groups subsequently collaborated on further characterization
220 and improvements of the TORM, and on an Arctic field deployment. In this paper, unless otherwise
221 noted, we report experimental results from the CU instrument. In cases where results from the FMI
222 instrument are reported, those are identified as FMI data. Experimental results from the CU and
223 Helsinki instruments were compared throughout the instrument development. The comparison of
224 results and the consistency in performance between the two instruments can be considered further
225 evidence for in the reproducibility of the TORM performance.

226

227 **2. Methods**

228

229 The basic principle of the ozone reactivity determination of biogenic emissions is illustrated in Fig.-1.
230 Emissions from vegetation are combined with a flow of ozone-enriched air and allowed to react in a flow

231 reactor. -Ozone is measured upstream and downstream of the reactor with a single instrument. In the standard
232 configuration of an UV absorption ozone monitor, ozone-containing air and scrubbed air (ozone-free air) are
233 either measured sequentially (one optical cell) or in

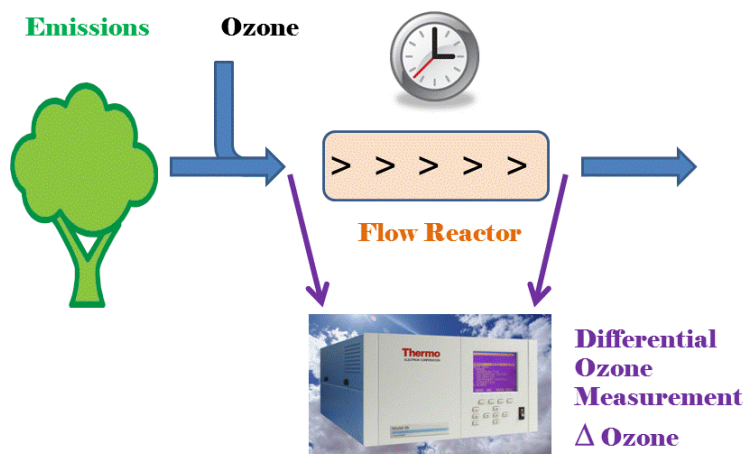
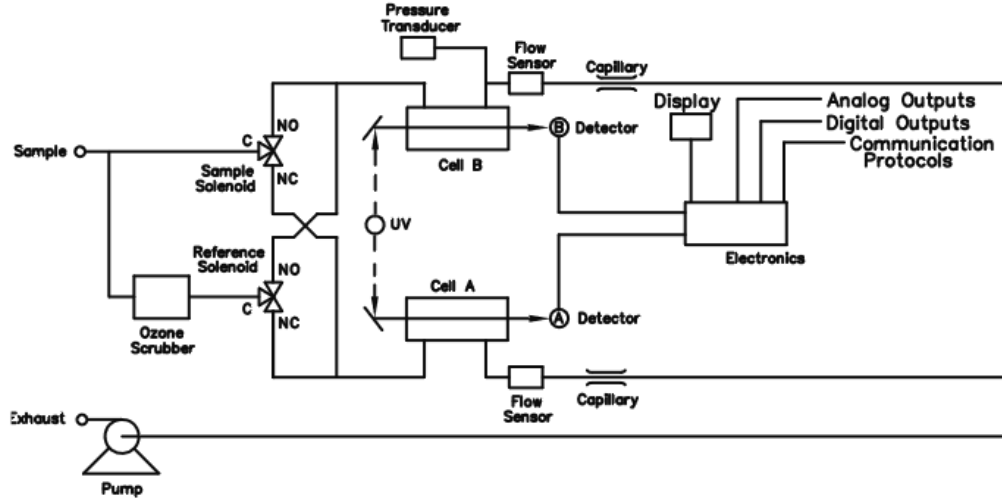


Figure 1

~~Principle of ozone reactivity measurement of biogenic emissions with one monitor that is configured for differential ozone signal recording.~~

234
235
236
237 parallel (two cell instruments), with the ozone mole fraction then determined following the Beer-Lambert
238 Law. The ozone mole fraction is proportional to the natural logarithm of the light intensity I divided from the
239 sample air (flow 1) by the light intensity in the scrubbed air I_0 (flow 2). By replacing the scrubbed air flow
240 path with a second sampling inlet line, the resulting signal no longer reflects the difference in ozone between
241 the sample (1) and scrubbed air (2, zero ozone), but instead becomes the difference in ozone between the two
242 sample flows (2-1). The required instrument modification is rather simple, illustrated in Fig. 2 for a Thermo
243 Scientific Model 49i instrument. It requires removal of the ozone scrubber (MoO scrubber in most cases) and
244 the separation of the scrubbed and sample air into two separate inlets. In the standard configuration, the 49i
245 samples air at $\approx 1.2 \text{ L min}^{-1}$ through one inlet. In the modified configuration, this flow is split in half to ≈ 0.6
246 L min^{-1} each for the Sample 1 and Sample 2 inlets. An early configuration of the experiment to illustrate how
247 the differential ozone monitoring was evaluated against the monitoring of ozone up and downstream of the
248 reactor with two instruments is presented in

(A) Original Plumbing Configuration



(B) Differential Ozone Monitoring Plumbing Configuration

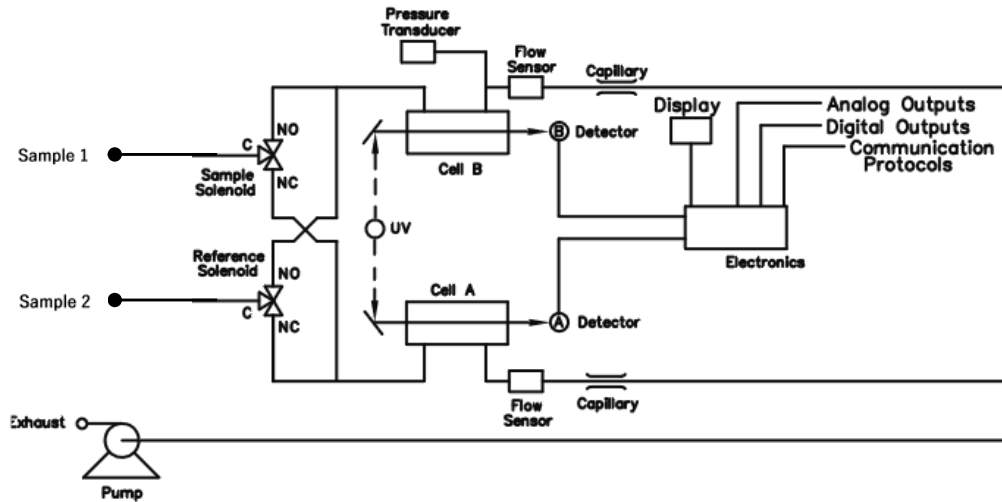


Figure 2

Plumbing configuration of a Thermo Scientific Instruments model 49 ozone UV absorption monitor in its original configuration (top) and in the modified configuration (bottom) for monitoring of ozone differentials.

249
250

251 Supplement C; the final one-monitor TORM configuration is shown in Fig. 3. The direct differential
252 ozone measurement was always conducted with a Thermo Scientific Model 49i monitor. During the
253 evaluation experiments, several different UV absorption ozone monitors were used for comparing
254 the direct measurement with a result from two individual instruments. Those included Thermo
255 Scientific Model 49i, Model 49C, and a MonitorLabs model 8810 monitor. The ozone that was added
256 upstream of the reactor was generated by the Thermo Scientific 49i instrument (with ozone generator
257 option) to yield a target ozone mole fraction of 100 ppb. To determine the proper ozone output from
258 the generator, an additional ozone monitor was temporarily sampling the air downstream of the
259 mixer. The ozone monitor was removed after dialling the ozone output to the target level and
260 monitoring it for several days and assuring its constant output.

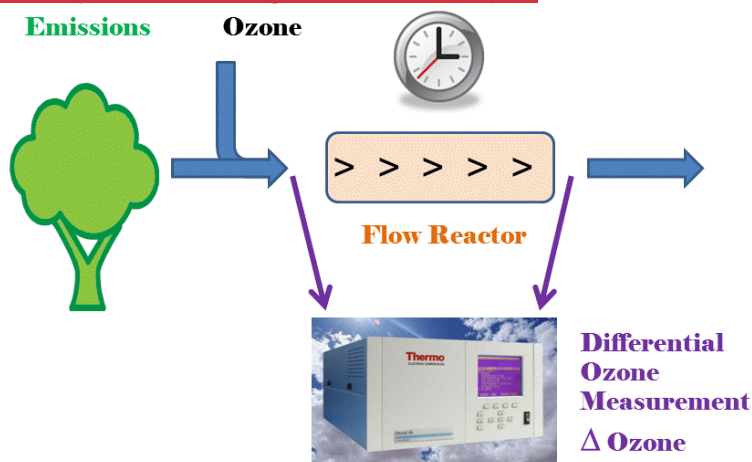
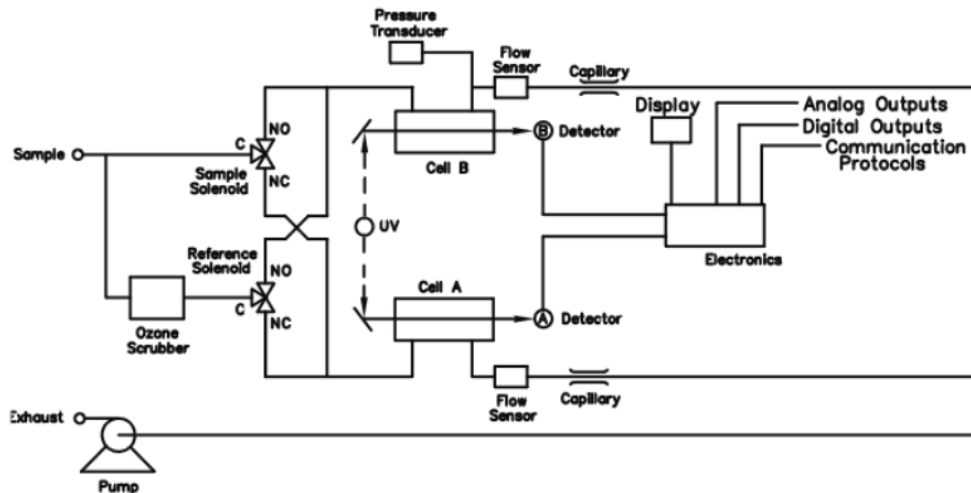


Figure 1. Principle of ozone reactivity measurement of biogenic emissions with one monitor that is configured for differential ozone signal recording.

(A) Original Plumbing Configuration



(B) Differential Ozone Monitoring Plumbing Configuration

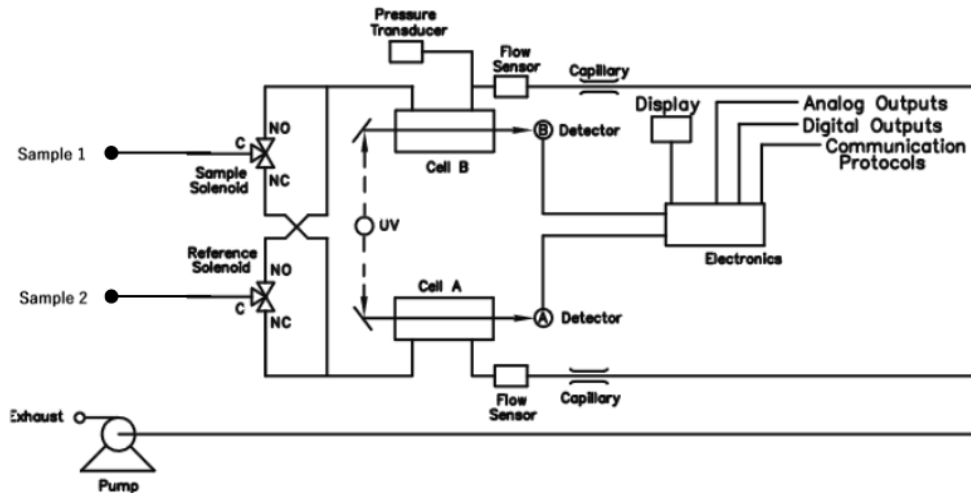


Figure 2. Plumbing configuration of a Thermo Scientific Instruments model 49 ozone UV absorption monitor in its original configuration (top) and in the modified configuration (bottom) for monitoring of ozone differentials.

261 While other studies [Matsumoto, 2014; Sommariva et al., 2020][Matsumoto, 2014; Sommariva et
262 al., 2020] utilized linear flow reactors, this experiment relied on using four glass flasks that were
263 plumbed in series. The glass flask reactor design was chosen because it was deemed more compact
264 and robust for field deployment applications. The 2.5 L borosilicate flasks that were used are air
265 sampling flasks that are routinely deployed in the NOAA Cooperative Sampling Network for the global
266 sampling of greenhouse gases. These glass flasks have been developed and extensively tested for
267 their inertness and purity towards atmospheric trace gases
268 (<https://www.esrl.noaa.gov/gmd/ccgg/flask.html>; flasks are fabricated by Allen Scientific, Boulder,
269 CO). Flasks are covered with shrink tubing as a protective film (polyolefin shrink wrap,
270 buyheatshrink.com) and have two ports with stopcock Teflon valves. ~~One~~The valve in the center of
271 the flask (Fig. 4) connects to a dip tube that leads to the inside ~~and~~ the opposite side end
272 of the flask ~~(Fig. 4)~~. This configuration allows efficient purging and replacement of the air volume inside the
273 flasks with minimal mixing. The flasks were plumbed such that the inflowing air was always
274 introduced through the dip tube. The four flasks in series add up to a total ≈ 10 L reactor volume, so
275 that the resulting residence time in the reactor is causing a sufficiently large differential signal (see
276 also section 3.5). The flasks are contained in ~~an~~ a 45 cm x 45 cm x 45 cm (inside dimension) Pelican

277 model 0340 cube case (Torrance, CA) that was fitted with 5 cm foam insulation on the inside. A rope
278 heater, temperature probe, and temperature controller allow to thermostatically control the
279 temperature, typically to ~~40°C~~40°C. With this heating, losses of VOCs in the reactor's flasks are
280 therefore less likely in comparison to the surfaces of a branch enclosure, for example, and the tubing
281 of the sampling line, which are all at ambient temperature. The ozone reactant gas was provided
282 from the Thermo Scientific 49i monitor using its integrated ozone generator. The output was set to
283 provide a 1000 ppb constant output, so that the 1:10 dilution with the sample air flow resulted in a
284 100 ppb ozone mole fraction entering the reactor. All experiments described in this paper were
285 conducted at this 100 ppb ozone mole fraction, unless stated otherwise. A mixer made of Teflon
286 material (7.50 mm OD, with 30 mixing elements, 22.5 cm length, Stamixco AG, Wollerau,
287 Switzerland) was inserted ~~upstream~~downstream of the introduction of the ozone gas flow for
288 providing turbulent mixing between the sample air and ozone-enriched air. All tubing was made of
289 6.4 mm o.d./4.7 mm i.d. PFA tubing.

290 The volume of the mixer and the tubing where the sample is mixed with ozone is only of about 15
 291 ml, so that any ozone loss occurring in the tubing is negligible compared to the much longer
 292 residence time in the much larger reactor volume. The instrument operation and signal acquisition
 293 were controlled via a National Instruments digital input interface and custom-written LabView
 294 software.
 295

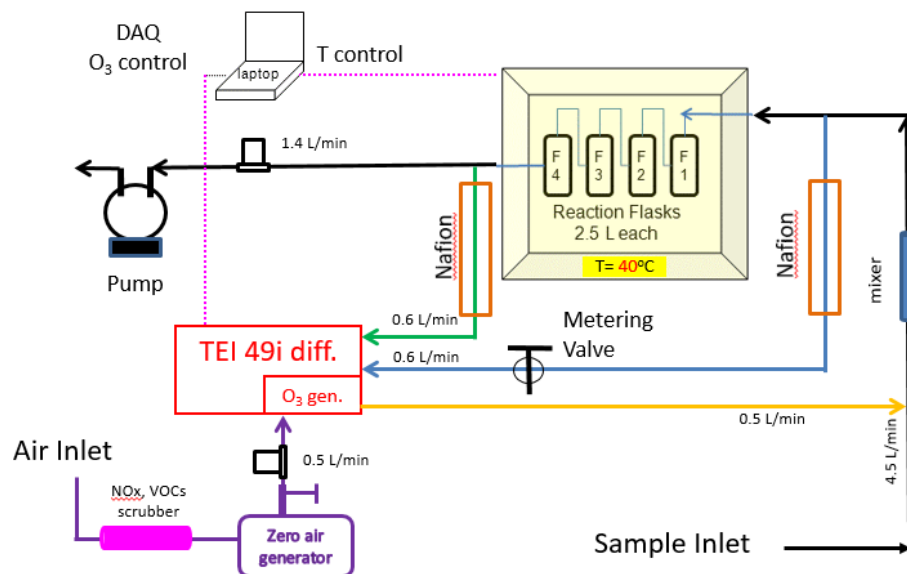


Figure 3

Final configuration of the total ozone reactivity monitor (TORM) using one Thermo Scientific (TEI) 49i-PS monitor plumbed for the direct differential ozone measurement (Figure 2), and with the Nafion dryers and metering valve included. Flow rates are indicated in the figure. Total flow through the reactor is 5 L min⁻¹.

296
 297

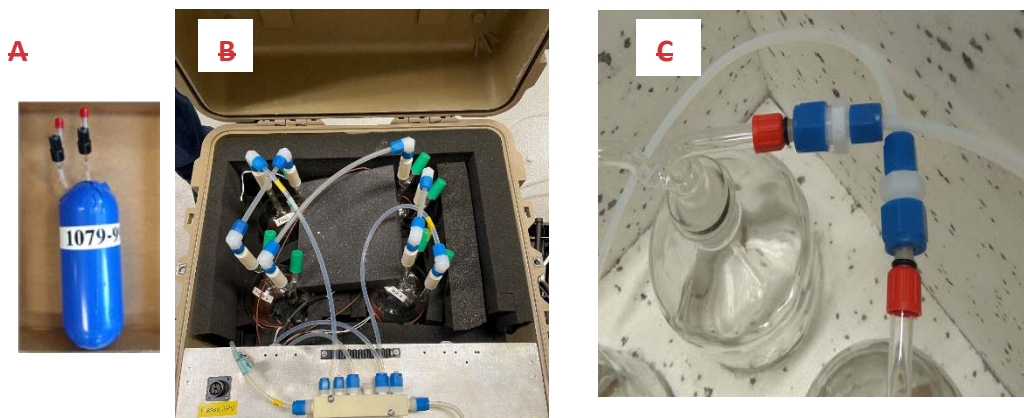


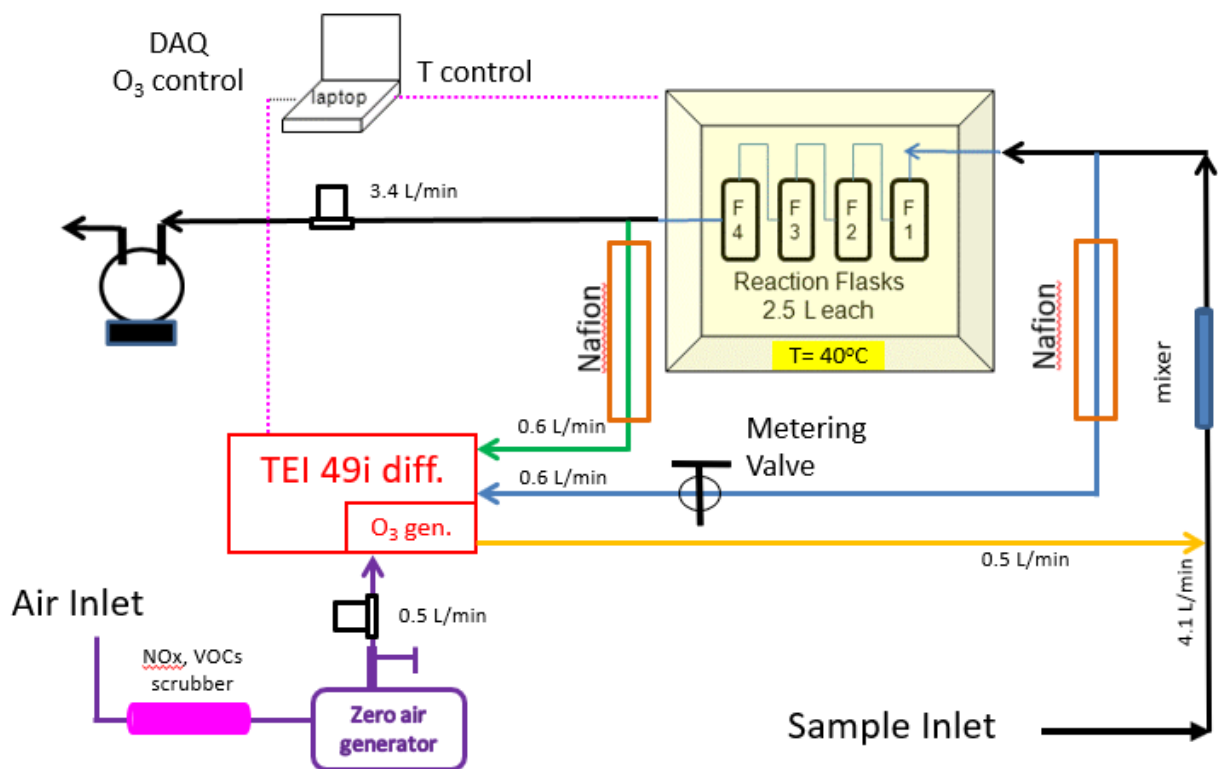
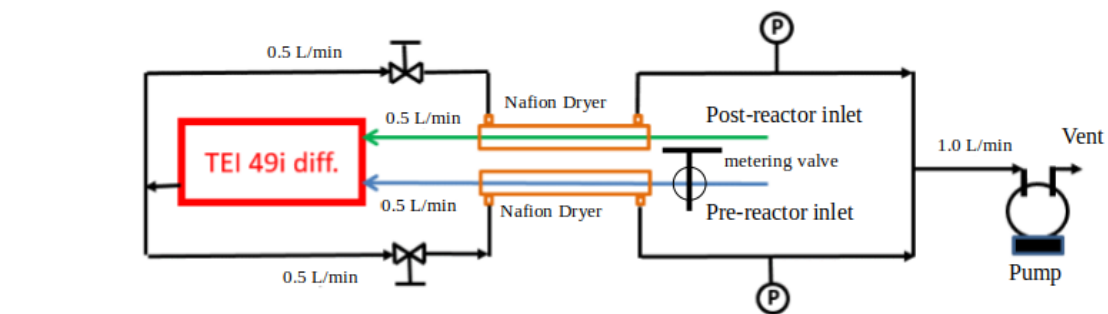
Figure 4

(A) Photograph of one of the glass flasks that were used for the University of Colorado, Boulder flow reactor. (B) The ozone reactor with four of the flasks plumbed in series contained in an insulated and temperature-controlled field-deployable enclosure. Four flasks were plumbed in series for a total flow reactor volume of 10 L. (C) The 2-L bottles (borosilicate glass 3.3) used in the Finnish flow reactor system.

298
 299

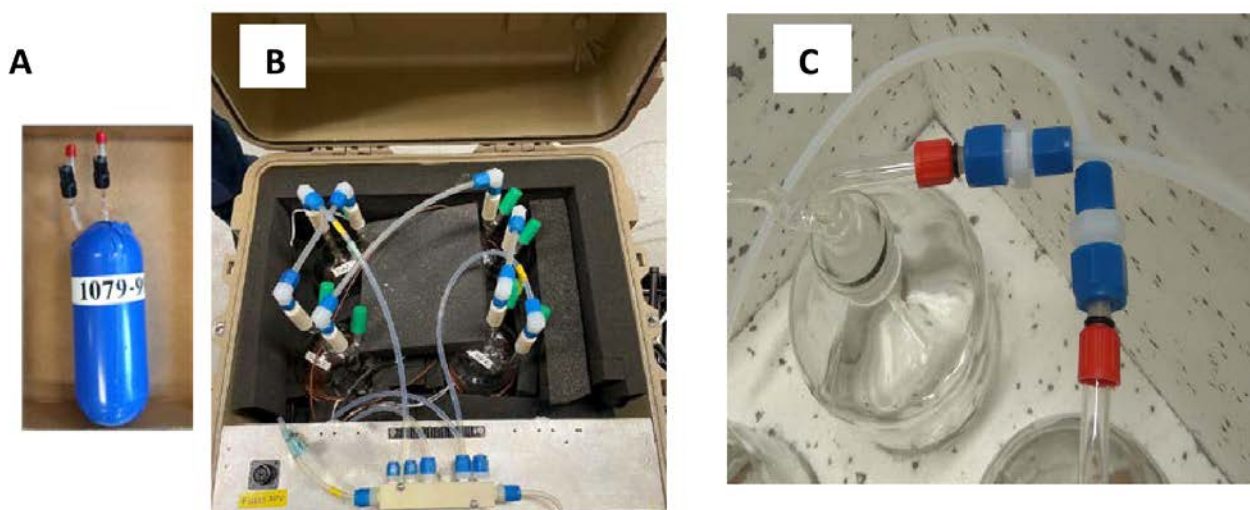
A

B



301

Figure 3. (A) Final configuration of the total ozone reactivity monitor (TORM) using one Thermo Scientific (TEI) 49i PS monitor plumbed for the direct differential ozone measurement (Figure 2), and with the Nafion dryers and metering valve included. Flow rates are indicated in the figure. Total flow through the reactor is 4 L min^{-1} . Please note that for simplicity this drawing does not show a second ozone monitor that was used for sampling the inflowing air between the mixer and the reactor to measure the ozone going into the reactor and setting the proper ozone output of the TEI 49i ozone generator. (B) Detail of the Nafion Dryer plumbing including the external pump that was added to the system for providing the purge flow for the Nafion dryers.



302

Figure 4. (A) Photograph of one of the glass flasks that were used for the University of Colorado flow reactor. (B) The ozone reactor with four of the flasks plumbed in series contained in an insulated and temperature-controlled field-deployable enclosure. Four flasks were plumbed in series for a total flow reactor volume of 10 L. (C) The 2-L bottles (borosilicate glass 3.3) used in the flow reactor system from FMI.

303

304 Experiments did not consider adding an OH scavenger (i.e. cyclohexane) [Matsumoto, 2014;
 305 Sommariva et al., 2020]. Sommariva et al. [2020][Matsumoto, 2014; Sommariva et al., 2020].
 306 Sommariva et al. [2020] estimated a < 6 % difference in ozone reactivity for BVOC ozonolysis
 307 reactions based on modeling, but could not identify differences with and without cyclohexane added
 308 in their experiments. It is therefore unlikely that addition of an ~~ozone scrubber~~OH scavenger will
 309 make a notable difference in the ozone reactivity monitoring results. ~~The instrument operation and~~

310

311 ~~A simple box model was used to estimate the expected differential signal acquisition were controlled~~
 312 ~~via a National Instruments digital input interface and custom written LabView software from a~~
 313 ~~known sample composition. It consists of reactions of the known BVOCs with O₃ which are solved~~
 314 ~~using the kinetics pre-processor (KPP; Damian et al. [2002]). The decay of ozone after the~~
 315 ~~corresponding residence time is compared to the background corrected differential signal~~
 316 ~~(Supplement B).~~

317

318 During field deployments, branch enclosures were set up on sweetgum (Liquidambar styraciflua L.),
 319 white oak (Quercus alba), and loblolly pine (Pinus taeda) tree branches following our previously
 320 described protocol [Ortega and Helmig, 2008]. [Ortega and Helmig, 2008]. A Tedlar bag (36" x 24" x
 321 24") was wrapped around a tree branch ~~of the size that when the bag is inflated,~~ the branch was
 322 situated in the middle of the bag with minimum touching of the wall. Scrubbed ambient air free of
 323 NO_x, ozone, and BVOC (Purafil and activated charcoal scrubbers), was delivered to the enclosure

324 at 25 L min⁻¹. Most of the moisture in the purge air was also removed by ~~passing~~condensing it
325 ~~through~~in a set of coils placed inside a refrigerator. The scrubber system did not remove carbon
326 dioxide. Air samples from the enclosure were taken through the ports affixed on the Tedlar bag,
327 drawn at flow rates that are suitable for the sampling apparatus and instruments. The rest of the
328 purge air escaped the enclosure mainly through the gap between the bag and the main stem of the
329 branch.

330

331

332 **3. Results and Discussion**

333

334 **3.1 System conditioning**

335

336 A newly assembled system exhibited a significant ozone sink, on the order of 20-30 ppb loss of
337 ozone (at 100 ppb) at a 54 L min⁻¹ reactor flow. The slow decline of the ozone loss signal over time
338 indicated a gradual equilibration of the system to the ozone in the sample air. This ozone loss ~~and~~was
339 most likely due to reaction of ozone with impurities and active sites on interior surfaces of the tubing
340 and reactor vessel. Therefore, we chose to label it as ozone wall loss (OWL). The OWL and its signal
341 drift could almost entirely be eliminated thorough conditioning of all tubing and the reactor with an
342 air flow enriched in ozone. For this conditioning, the system was purged for 24 hours with 500 ppb
343 of ozone. After this treatment, the ~~ozone loss~~OWL associated with the sample flow through the
344 reactor in the absence of chemical gas reactants, i.e. the reactor background signal, was, depending
345 on the particular system condition and operational variables, on the order of 1-2 % of the supplied
346 ozone mole ~~fractions~~fraction; i.e. at 100 ppb ozone, the loss was reduced to 1-2 ppb and did no
347 longer show any drifts in the signal. ~~After warmup, the 1 min averaged $\Delta[\text{O}_3]$ signal displayed a~~
348 ~~standard deviation (σ) of 0.075 - 0.096 ppb (over 1 h, n = 60). This translates into a limit of detection~~
349 ~~(3σ) of $1.8 - 2.3 \times 10^{-5} \text{ s}^{-1}$ for the reactivity (for a theoretical residence time of 150 s, and correcting~~
350 ~~for the ozone dilution flow). This sensitivity is slightly higher, i.e. resulting in a lower limit of detection~~
351 ~~than that reported by [Matsumoto, 2014] ($4 \times 10^{-5} \text{ s}^{-1}$, for a residence time of 57 s), and~~
352 ~~approximately 2-3 times lower than that reported by [Sommariva et al., 2020] ($4.5 - 9 \times 10^{-5} \text{ s}^{-1}$ for a~~
353 ~~residence time of 140 s). The stability of the ozone reactivity signal was tested on the Finnish system~~
354 ~~over a full day, with the reactor located outside and sampling from an empty enclosure that was~~The
355 OWL recorded after system conditioning (i.e., wall losses) can be different if the system is run in a
356 different configuration (e.g., different flow through the reactor, different temperature or relative
357 humidity).

358

359 The limit of detection (LOD) for the ozone differential signal was determined from the stability of the
360 differential signal with the FMI instrument. The experiment was conducted over a full day, with the
361 reactor located outside and sampling from an empty enclosure that was purged with clean, BVOC-
362 free air and subjected to a full daily cycle of changing ambient conditions in temperature, humidity,
363 and light. There was no notable drift in the $\Delta[\text{O}_3]$ signal over the measurement period despite the
364 changes in the environmental conditions (Supplement D). After warmup, the 1-min averaged $\Delta[\text{O}_3]$
365 signal displayed a standard deviation (σ) of 0.075 - 0.096 ppb (over 1 h, n = 60), which corresponds
366 to a (3σ) LOD of 0.23-0.29 ppb.

367

368 Using equation (S6) from Supplement A and taking into account the dilution of sampled air with the
369 added O_3 flow, the LOD for the ozone reactivity determination can be calculated from this (3σ) signal.
370 It results in a value of $1.8 - 2.3 \times 10^{-5} \text{ s}^{-1}$. The calculation assumes an ozone mole fraction of 100

371 ppb before the reactor and a residence time of 150 s. Other systems to measure the ozone reactivity
372 using two separate monitors before and after the reactor reported slightly higher (i.e. less sensitive)
373 limits of detection, i.e. $4 \times 10^{-5} \text{ s}^{-1}$ [Matsumoto, 2014], and $4.5 - 9 \times 10^{-5} \text{ s}^{-1}$ [Sommariva et al., 2020].
374
375

376 **3.2 Balancing of the ozone monitor inlet pressures**

377

378 The readings from the differential ozone monitor are sensitive to the difference in the pressure in the
379 two sampling lines that connect to upstream and downstream of the reactor (Supplement E). The
380 pressure differential results from the vacuum generated by the sampling pump for providing flow
381 through the reactor. The 49i diagnostics menu allows monitoring of the pressures of the two optical
382 cells. In the original configuration, it was found that there was a pressure difference of, depending of
383 the flow rate, 20-30 torr between the two cells at a 54 L min⁻¹ reactor flow, with the lower pressure
384 recorded in the line downstream of the reactor. This pressure differential alters between negative
385 and positive values as the monitor alternates air from the two inlets through the two optical cells.
386 This pressure difference results in an artificial ozone signal offset between the two sampling paths.
387 An increase of the flow rate through the reactor causes a change in the pressure difference and the
388 ozone differential reported by the monitor: Increasing the flow rate from 2 to 9 L min⁻¹ corresponded
389 to an increase from 2 to 7 ppb increase in the differential ozone signal. This behavior is clearly a
390 measurement artifact and counter to the expected ozone loss, as the actual chemical ozone loss
391 decreases with decreasing residence time of the air inside the reactor (i.e. increasing flow rate). This
392 measurement artifact was mitigated by inserting a 0.64 cm Teflon metering valve into the sampling
393 line upstream of the reactor. By closing the valve slightly, the flow was restricted to where both cell
394 pressure readings from the reactor were equal (within ≈ 1 torr). This resulted in an ozone differential
395 signal of ≈ 1.7 ppb that was insensitive to the reactor flow rate (Supplement E). The final plumbing
396 configuration of the TORM and its integration into a vegetation enclosure experiment is shown in Fig.
397 5.
398

399 **3.3 Evaluation of the direct differential ozone reactivity measurement**

400

401 Results from the parallel operation of two ozone monitors measuring the actual ozone before and after
402 the reactor, with $\Delta[\text{O}_3]$ calculated from the difference of the two readings, compared to the direct ozone
403 differential measurement by TORM are summarized in Fig. 6. Field data, collected during the Southern
404 Oxidant and Aerosol Study (SOAS) (CU Boulder system), constitute a total of ten days of measurements
405 collected using branch enclosures on three different branches of sweetgum trees. The OWL to the TORM was
406 determined on five occasions by sampling from an empty bag. In these field conditions, the background
407 differential signal (3-5 ppb, Fig. 6B) was somewhat higher than in the laboratory experiments described in the
408 previous section. The OWL results bracketing the vegetation enclosure experiments were averaged and
409 subtracted from the recordings of the enclosure experiments in between. The ozone differential was normalized
410 to the air flow through the chamber and to the dried weight of leaf biomass that was sampled from the
411 vegetation in the branch enclosure. These time series data show a clear diurnal cycle with the ozone
412 reactivity differential increasing steeply during daytime hours. Results are reasonably consistent between days
413 and the three different enclosures, considering that the BVOCs emissions that determine this signal are highly
414 sensitive to light and the enclosure temperature, which varied during the experiment. There is high agreement
415 between the ozone reactivity $\Delta[\text{O}_3]$ results from both configurations across these experiments. A linear

416 regression between results from the two monitoring methods from the SOAS study yields a slope value of
 417 0.996. The graphed data also show the substantial improvement in the noise of the measurement with the direct
 418 differential monitoring (A, B). The precision error of the direct differential measurement is only about 1/5
 419 compared to the result from the two monitors. After the system equilibration, the 1- σ standard deviation of
 420 the differential ozone measurement for 1-min averaged readings was generally in the range of

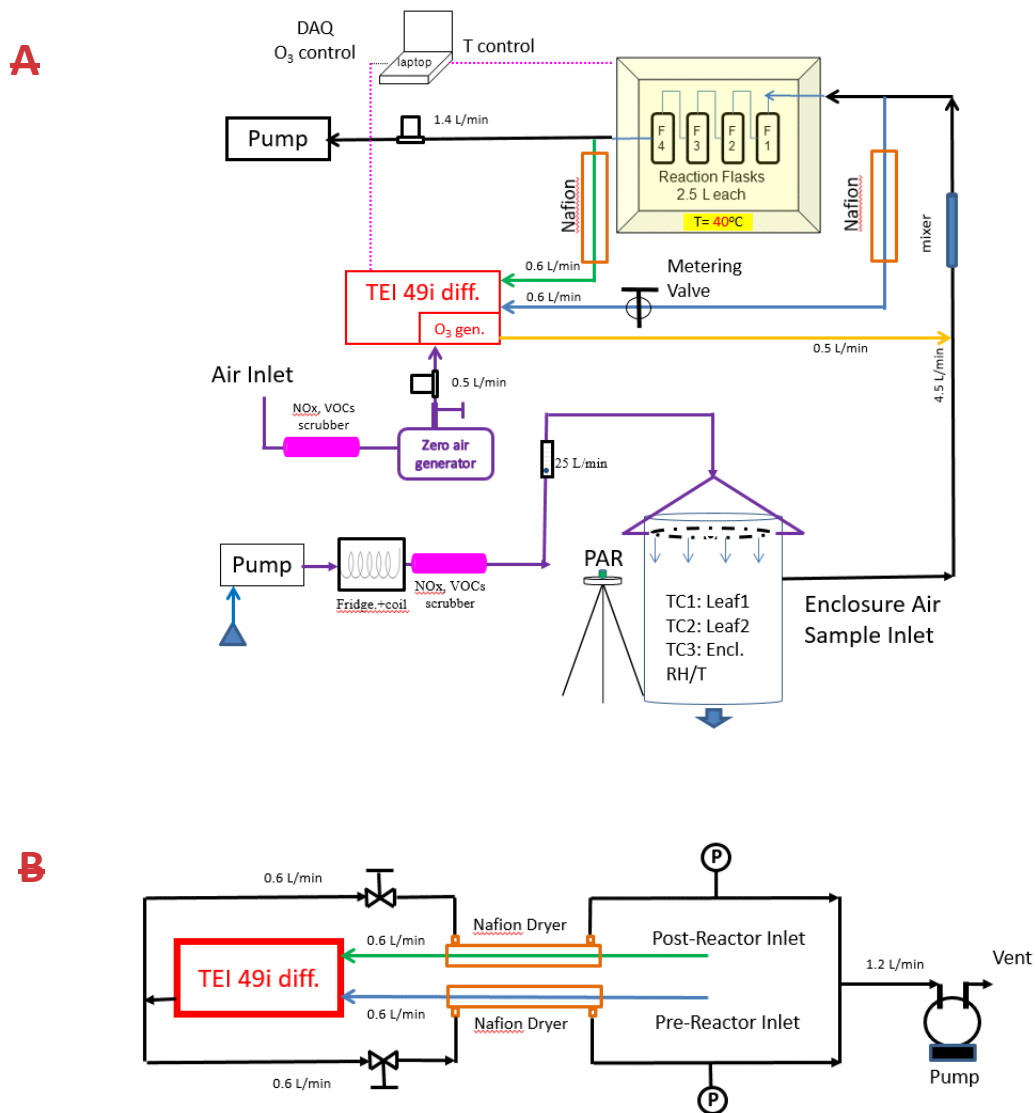


Figure 5

(A) Final configuration of the total ozone reactivity monitor with one differential ozone monitor, the sampling line pressure balancing valve, and the Nafion dryers. Schematic (B) shows the detail of the Nafion Dryer plumbing including the external pump that was added to the system for providing the purge flow for the Nafion dryers.

421

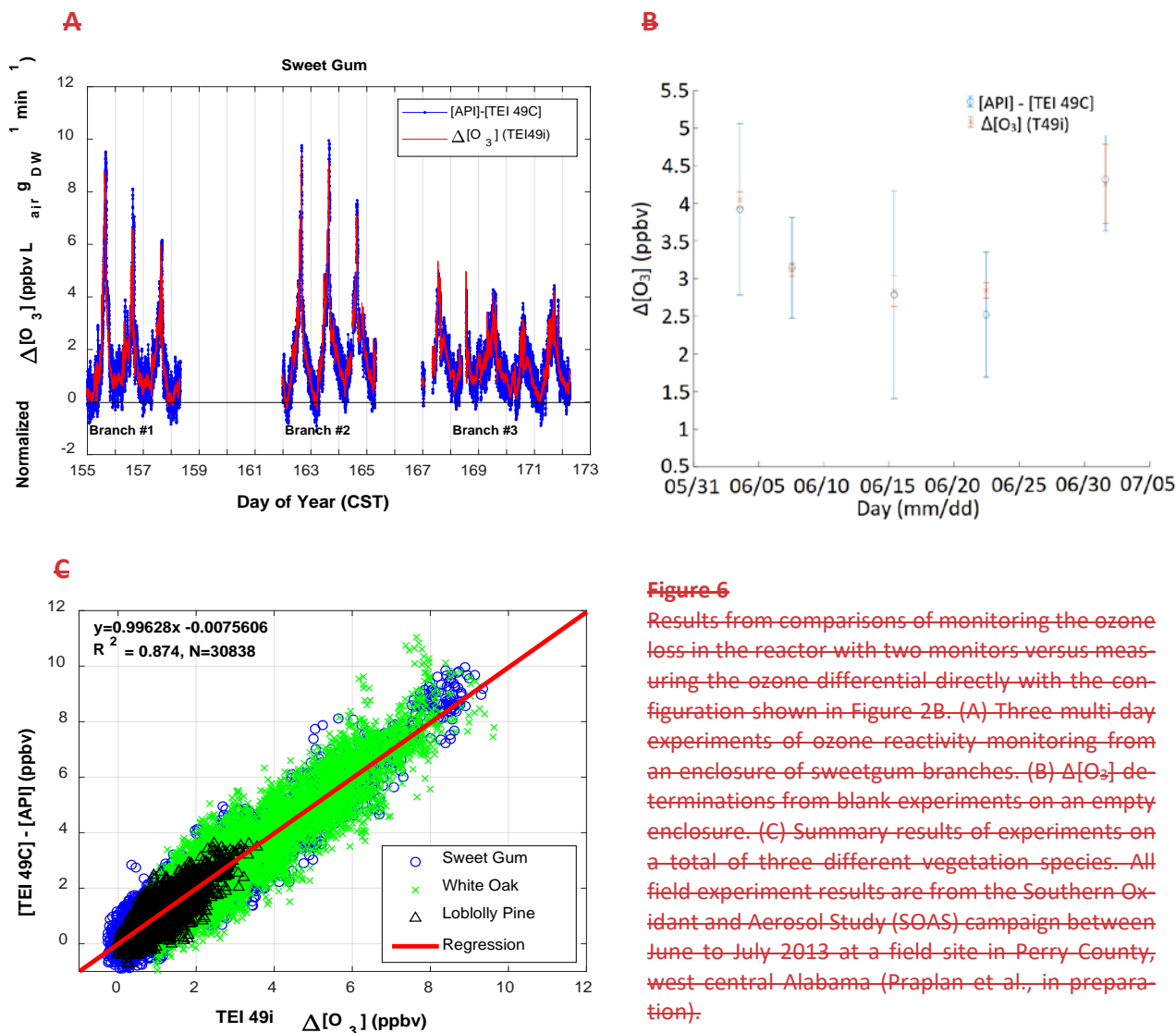


Figure 6

Results from comparisons of monitoring the ozone loss in the reactor with two monitors versus measuring the ozone differential directly with the configuration shown in Figure 2B. (A) Three multi-day experiments of ozone reactivity monitoring from an enclosure of sweetgum branches. (B) $\Delta[O_3]$ determinations from blank experiments on an empty enclosure. (C) Summary results of experiments on a total of three different vegetation species. All field experiment results are from the Southern Oxidant and Aerosol Study (SOAS) campaign between June to July 2013 at a field site in Perry County, west central Alabama (Praplan et al., in preparation).

422

0.1 – 0.2 ppb, which was 2-3 times lower than the calculated ozone difference from the two-monitor measurement. These results clearly indicate the benefits of the single monitor measurement: (1) the accuracy of the ozone reactivity measurement differential signal is consistent with the differential two-monitor determination; (2) there is a very significant improvement in the measurement precision from using a single monitor; and (3) the operation of a single monitor is less tedious and labor intensive as it does not require the regular intercomparison for determination of offsets and drifts and correction algorithms for calibrating the response of two individual monitors [Bocquet et al., 2011; Sommariva et al., 2020]. [Bocquet et al., 2011; Sommariva et al., 2020].

430

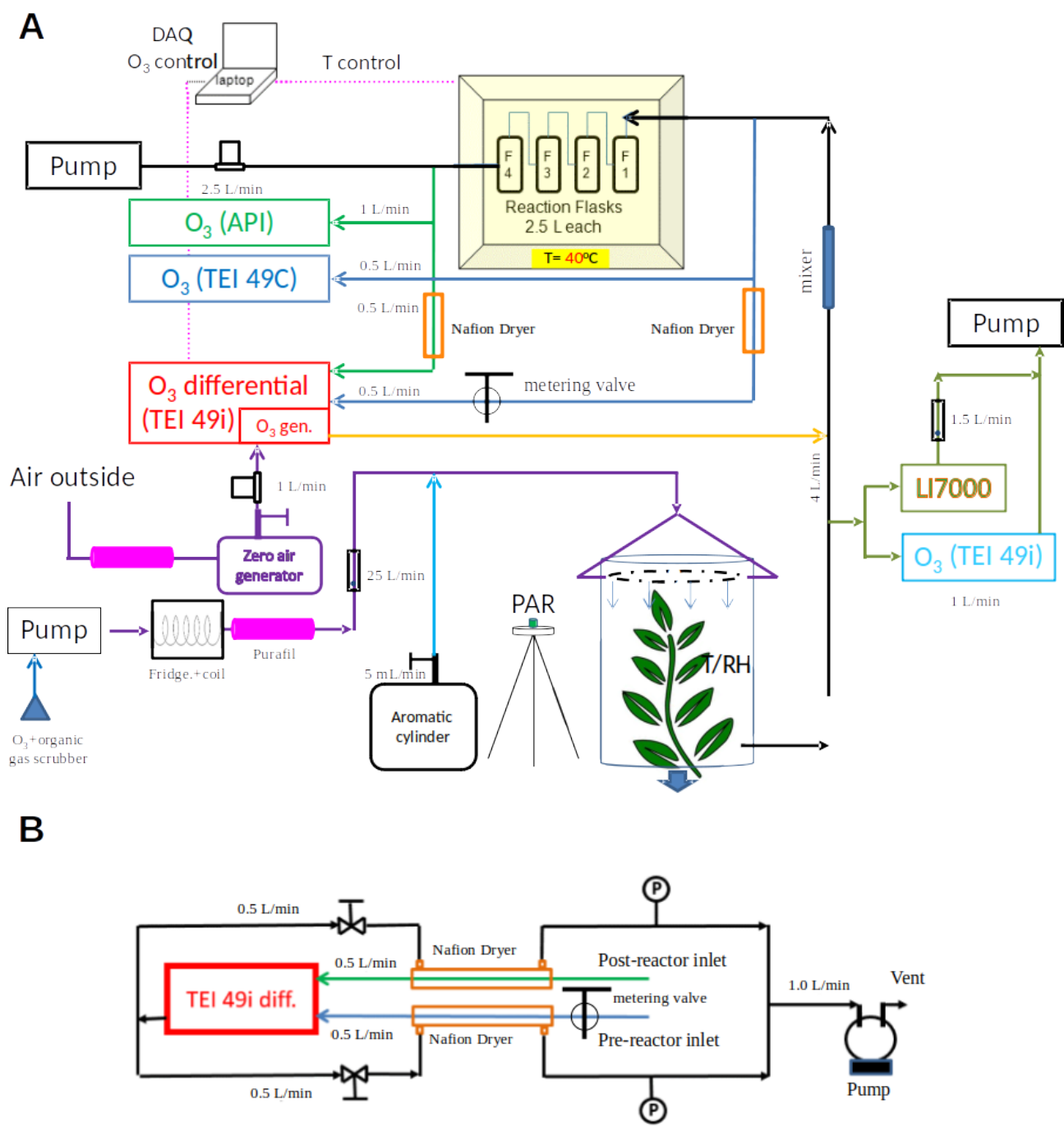


Figure 5. (A) Final configuration of the total ozone reactivity monitor with one differential ozone monitor, the sampling line pressure balancing valve, and the Nafion dryers. Note that this schematic does not include the purge flows required by the Nafion dryers. These are described separately in Figure 3B.

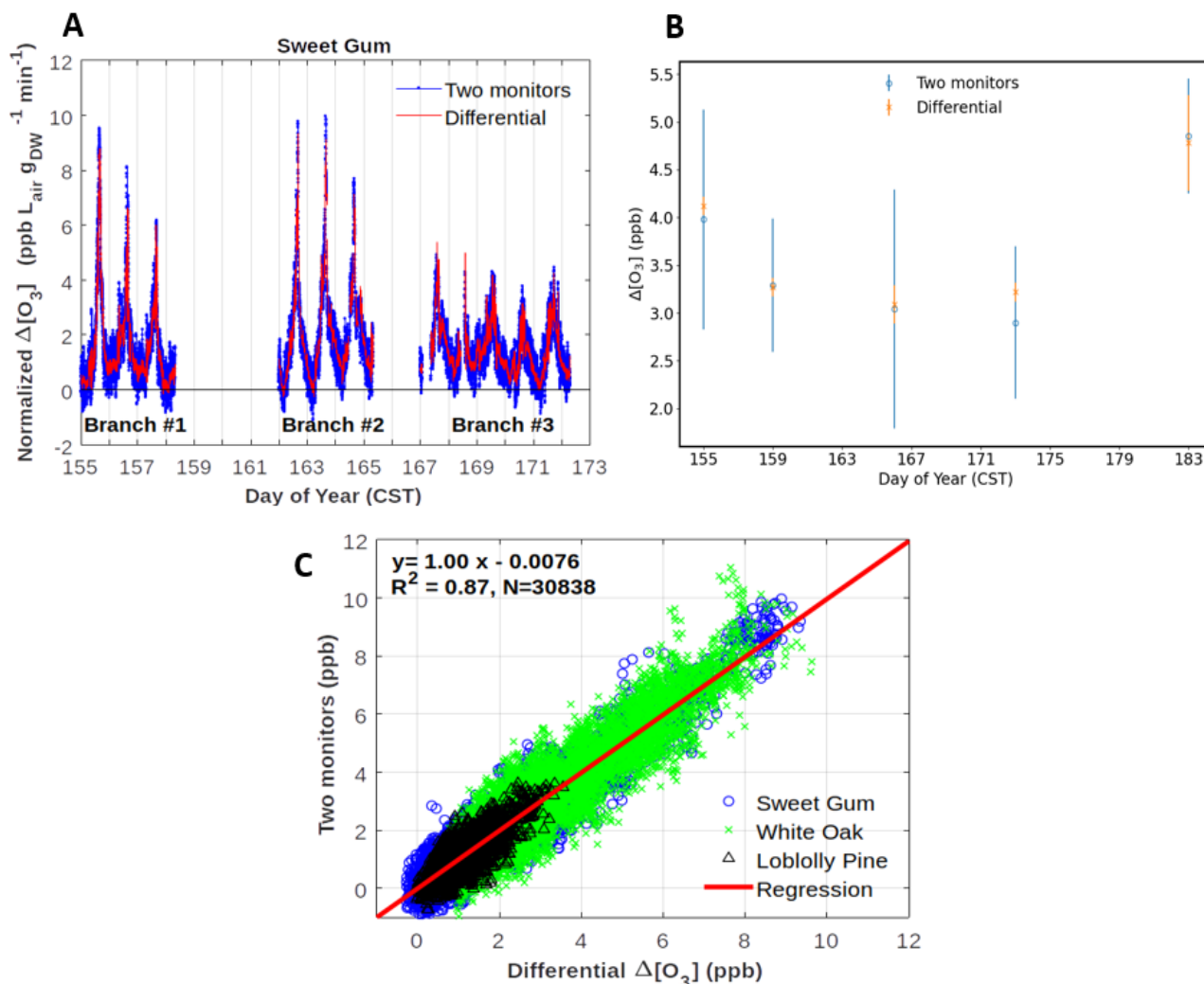


Figure 6. Results from comparisons of monitoring the ozone loss in the reactor with two monitors versus measuring the ozone differential directly with the configuration shown in Figure 2B. (A) Three multi-day experiments of $\Delta[\text{O}_3]$ monitoring from an enclosure of sweetgum branches, Data are also corrected for the empty bag OWL data shown in panel (B) and normalized for flow through the enclosure and dried weight of leaf biomass. (B) $\Delta[\text{O}_3]$ determinations from blank experiments on an empty enclosure. (C) Summary results of experiments on a total of three different vegetation species. All field experiment results are from the Southern Oxidant and Aerosol Study (SOAS) campaign between June to July 2013 at a field site in Perry County, west central Alabama (Praplan et al., in preparation).

431

432 3.4 Sample residence time in the reactor

433

434 The desired operation of a flow reactor system is for air to move through the reactor as a narrow
 435 plug, with minimal turbulence and mixing. Most flow reactors are tubular and linear and are used in
 436 laboratory settings. Depending on their operational variables, they achieve seconds to a few minutes
 437 residence time. The residence time and peak broadening during transport through the reactor was
 438 studied by installing a syringe injection port upstream of the reactor, injection of a small volume of a
 439 1 ppm standard of nitric oxide (NO), and monitoring the ozone loss from the ozone + NO reaction
 440 downstream of the reactor with a fast-response (5 Hz) nitric oxide chemiluminescence instrument.
 441 Experiments were conducted in two different configurations: -1. In the normal plumbing configuration,
 442 with the incoming air introduced to each flask through the dip tube. -2. To test the effect of the dip
 443 tube, the plumbing was also reversed. The flow through the reactor was set to 4 L min^{-1} , which for
 444 an ideal flow reactor, at 10 L volume, should result in a 2.4 min (150 s) residence time. Results of
 445 these tests are shown in Fig. 7. For both configurations, the peak signal was observed earlier than

446 the theoretical time, i.e. ≈ 3918 s for the normal configuration, and ≈ 50 s for the reversed
447 configuration. The peak widths (at half of peak maximum) were ≈ 90 s and 120 s, for the normal and
448 reversed configuration, respectively. The behavior in these data show that there is a considerable
449 amount of mixing inside the reactor glass flasks, causing deviation from an ideal flow reactor.
450 Nonetheless, the residence time of ≈ 120 -s for the normal plumbing configuration is sufficient to ~~meet~~
451 ~~the requirements for the allow~~ ozone ~~reaction experiment to react with the sample so that a large~~
452 ~~enough differential signal can be measured~~. The findings from this experiment were confirmed at a
453 higher, 6 L min^{-1} flow rate (Supplement F). Both experiments show the advantage of the air
454 introduction through the dip tube, resulting in a narrower peak, i.e. narrower defined residence time.

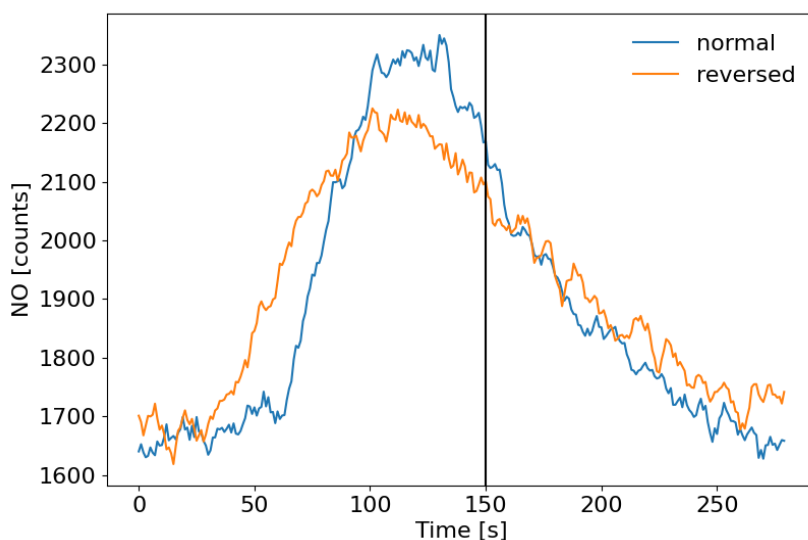


Figure 7

Test of sample air residence time in the flow reactor. A small volume of a 1 ppm NO standard was injected through a port upstream of the reactor and NO was monitored downstream with a fast response chemiluminescence analyzer (1 s time resolution). 5 s running averages are presented here. The normal configuration was with the flow entering each flask through the dip tube. The reversed configuration was with the air low exiting each flask through the dip tube. The vertical black line indicates the theoretical residence time based on the total flow rate (4 L min^{-1}) and total volume (10 L) of the reactor, assuming that there was no mixing inside the flasks.

455
456

457 For this configuration of the reactor, the mean residence time is about 90% of the theoretical
458 residence time. In case the flow through the reactor deviates from 4 or 6 l min⁻¹, at which these
459 experiments were conducted, a factor 0.9 is applied to the theoretical residence time in order to
460 estimate as best as possible the peak residence time for ozone reactivity calculations.

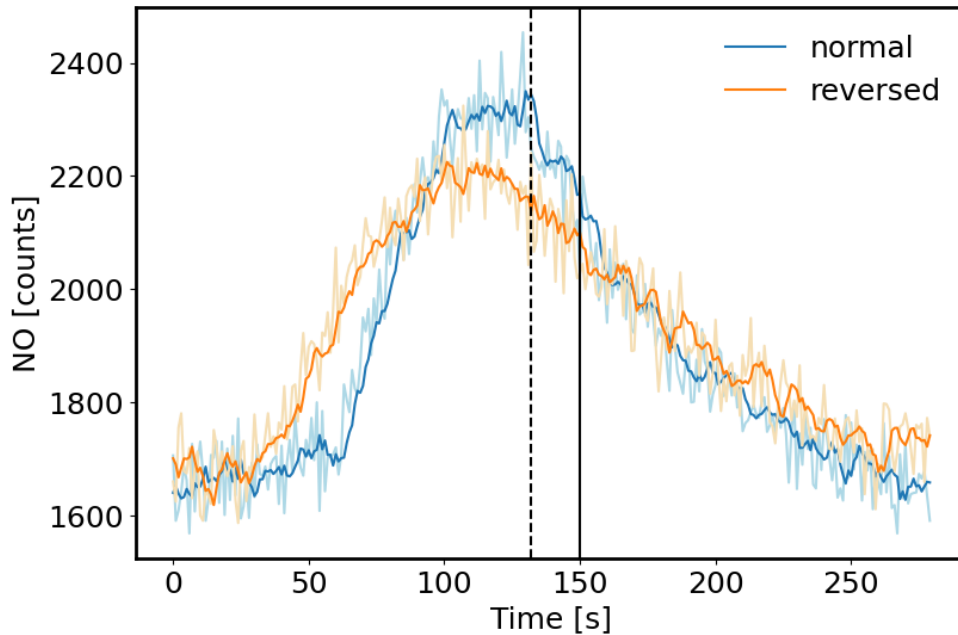


Figure 7. Test of sample air residence time in the flow reactor. A small volume of a 1 ppm NO standard was injected through a port upstream of the reactor and NO was monitored downstream with a fast response chemiluminescence analyzer (1 s time resolution). 5 s running averages are presented here. The normal configuration was with the flow entering each flask through the dip tube. The reversed configuration was with the airflow exiting each flask through the dip tube. The vertical black line indicates the theoretical residence time (150 s) based on the total flow rate (4 L min⁻¹) and total volume (10 L) of the reactor, assuming that there was no mixing inside the flasks. The dotted line depicts the mean of the distribution at 132 s for the normal configuration.

462

463

3.5 Evaluation and Mitigation of Humidity effects

464

465

466

467

468

469

470

471

472

473

474

475

476

477

478

479

480

481

482

483

484

As elucidated on in the introduction section, changes in humidity can severely interfere in the ozone determination. [Wilson and Birks, 2006; Spicer et al., 2010]. Ozone monitors have been found to be less sensitive, i.e. report ozone below its actual value at high humidity, and to exhibit large artificial signal fluctuations from rapid changes in the sample water vapor. Characterization and mediation of the sensitivity of the ozone reactivity measurement to water vapor was a main emphasis of our experiments. Earlier experiments, where the sampling flow was subjected to variable water vapor, such as by injecting small volumes of water through an injection port upstream of the reactor in the configuration shown in Supplement C, confirmed the findings from prior literature: Despite a constant ozone mole fraction that was fed into the reactor, both, the two-monitor determination, and the single monitor ozone differential determination, showed instantaneous changes in the ozone signal, reaching on the order of 10 ppb. ~~The~~This bias in the ozone recording lasted significantly longer (≈ 10 times) than the residence time that was determined in the above described experiment using nitric oxide. demonstrating that the retention of water, likely from reversible uptake to walls and tubing inner surfaces in the reactor, is longer, and flushing water vapor out of the reactor takes a higher purge volume than for less polar/more volatile gases. These water vapor effects on the ozone signal were mitigated by two modifications to the TORM: (1) the glass flasks reactor was insulated and a heater, regulated by a temperature controller was added to control the temperature of the reactor to 40°C-40°C. This heating significantly reduced the residence and interference time from the water injection, likely due to a reduction of the adherence of the water vapor to the walls of the glass flasks and other reactor components. Our observations agree with the findings reported by ~~Wilson and~~

485 ~~Birks [2006], Wilson and Birks [2006]~~, who found a reduction of the water interference for their 2B
486 Technologies ozone monitor when the glass optical cell was slightly heated; and (2) Nafion dryers
487 (0.64 cm o.d. x 180 cm length; MD-110-~~7272739~~ gas dryer, Perma Pure LLC, New Jersey, USA)
488 were inserted into both ozone monitor inlet flows before and after the reactor. We installed the two
489 Nafion dryers there, rather than one Nafion dryer for the sample flow path going into the reactor, to
490 prevent possible losses of polar and unsaturated compounds from the sample flow passing through
491 a Nafion dryer, as has been reported in other prior research. The purge flow for the Nafion dryers
492 was provided by the vent flow from the TEI 49i. The analyzer vent flow was split into two
493 approximately equal fractions, resulting in 0.6 L min⁻¹ flow for each Nafion Dryer (Figure 5B). Throttle
494 valves were installed in both lines as flow restrictors and adjusted such that the pressure in the
495 exterior chamber of the Nafion dryers was ≈10-% below the interior section of the dryer (cell pressure
496 readings from the differential 49i monitor). The Nafion dryers were conditioned using the same
497 protocol as for the reactor (see above), after which there was no notable ozone loss from sampling
498 the ozone-enriched air flow through the Nafion tubing, in agreement with other previous studies that
499 have reported negligible ozone loss in Nafion tubing materials ~~[Wilson and Birks, 2006; Boylan et al.,~~
500 ~~2014; Kim et al., 2020]~~. [Wilson and Birks, 2006; Boylan et al., 2014; Kim et al., 2020].

501
502 Results from an experiment with the Nafion dryers in use and where water vapor was increased in
503 multiple steps is shown in Fig. 8. The same humidification system as described by ~~Boylan et al.~~
504 ~~[2014]~~ Boylan et al. [2014] was used for moisturizing a zero air dilution gas fed to the TORM. The
505 resulting humidity was recorded with a LICOR model 7000 CO₂/H₂O gas analyzer downstream of
506 the mixer, but upstream of the reactor. Each humidity level was maintained for 30 min, before
507 subjecting the system to the next higher moisture level by a rapid change in the humidity generator
508 setpoint. The ~~ozone reactivity differential~~ signal was monitored with the differential 49i monitor, as
509 well as by recording the absolute ozone upstream and downstream of the reactor with two individual
510 monitors. Both ozone monitoring systems were sampling through the Nafion tubing. Results of the
511 experiment (Fig. 8) show a residual ~~ozone reactivity differential~~ signal response of ≈0.5 ppb over an
512 ~~≈~~ approximately 10 to 84 % RH span for the differential monitor. The two-monitor Δ[O₃] response is
513 approximately six times as large. The spikes seen during the moisture transition periods seen in
514 earlier experiments disappeared completely for the differential monitor. If background measurements
515 are performed at a different RH than the ozone reactivity measurements, this residual differential
516 signal needs to be taken into account on a case-by-case basis.

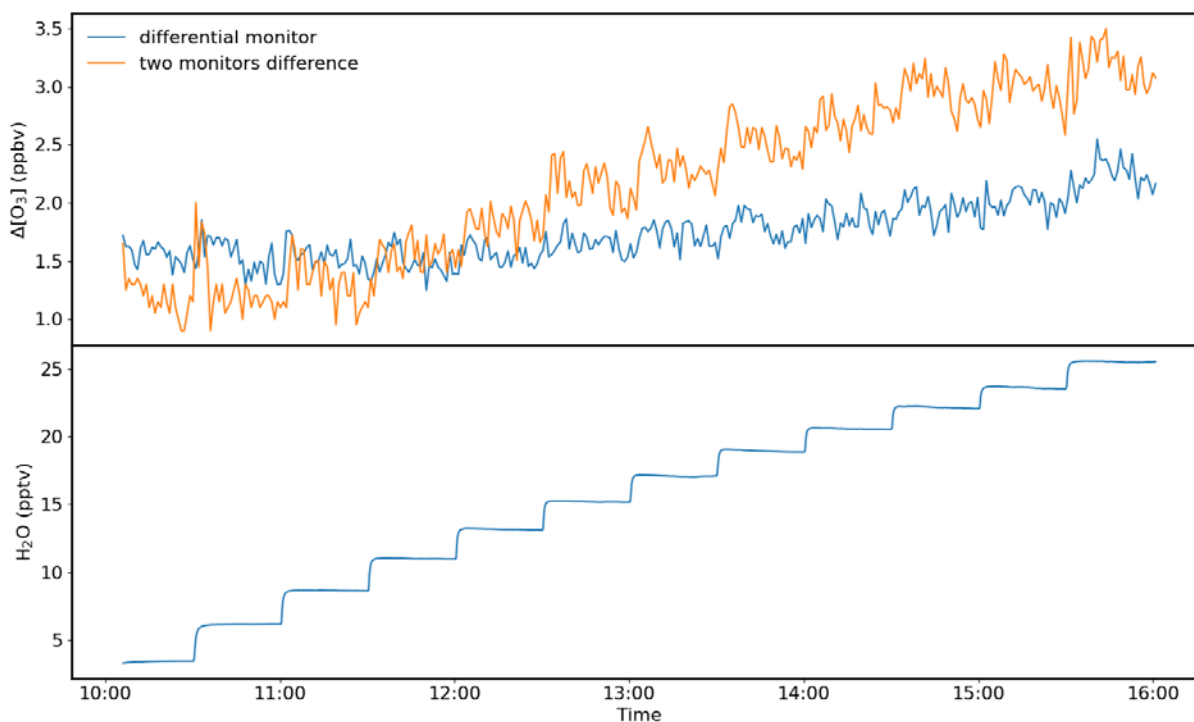


Figure 8

Experiment with increasing humidity in the air supplied to the TORM. The humidity content of the sample air is displayed in the lower graph in units of parts per thousand (ppt). A total of 12 levels were administered, from ~3–26 ppt, which at room temperature conditions (25°C) is approximately equivalent to a RH range of 10–84%.

517

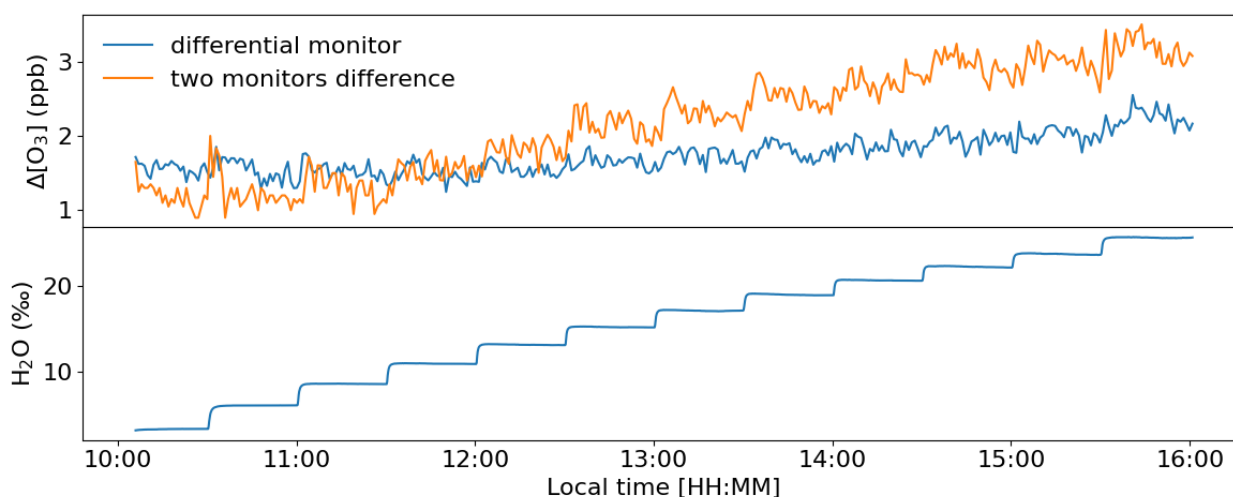


Figure 8. Experiment with increasing humidity in the air supplied to the TORM. The humidity content of the sample air is displayed in the lower graph in units of parts per thousand (‰). A total of 12 levels were administered, from ~3–26‰, which at room temperature conditions (25°C) is approximately equivalent to a RH range of 10–84%.

518

519 Similar order of magnitude results were obtained in a series of experiments where liquid water (20
520 to 100 μl) was injected into the sampling flow through a septum port upstream of the reactor. The

521 Nafion dryer removed $\approx 2/3$ of the water interference, and the differential monitor response to the
522 water injection was less than half compared to calculated difference from the two-monitors
523 configuration (Supplement G).

524

525 3.6 Application Examples

526

527 Ozone reactivity of test mixtures and samples from vegetation enclosures were investigated in laboratory
528 and field systems. A laboratory experiment using a flow of limonene standard is presented in Fig. 9. The
529 purpose of the experiment was to demonstrate the linearity of the TORM response and to derive a lower bound
530 estimate for the TORM response. Here, we chose to define the TORM response (in units of ppb s) as the delta
531 ozone signal (ppb) per unit of ozone reactivity (s^{-1}), as calculated from the product of the reactant mole fraction
532 and its ozone rate constant. The gas standard was prepared in house for a target mole fraction of 20 ppm.
533 However, the actual mole fraction is expected to have decreased with time, but could not be independently
534 verified at the time of the experiment. The ~~reported~~theoretical mole fractions, after mixing of the standard
535 with the dilution flow, range between 0–33 ~~ppbv~~ppb, which is a typical range

536

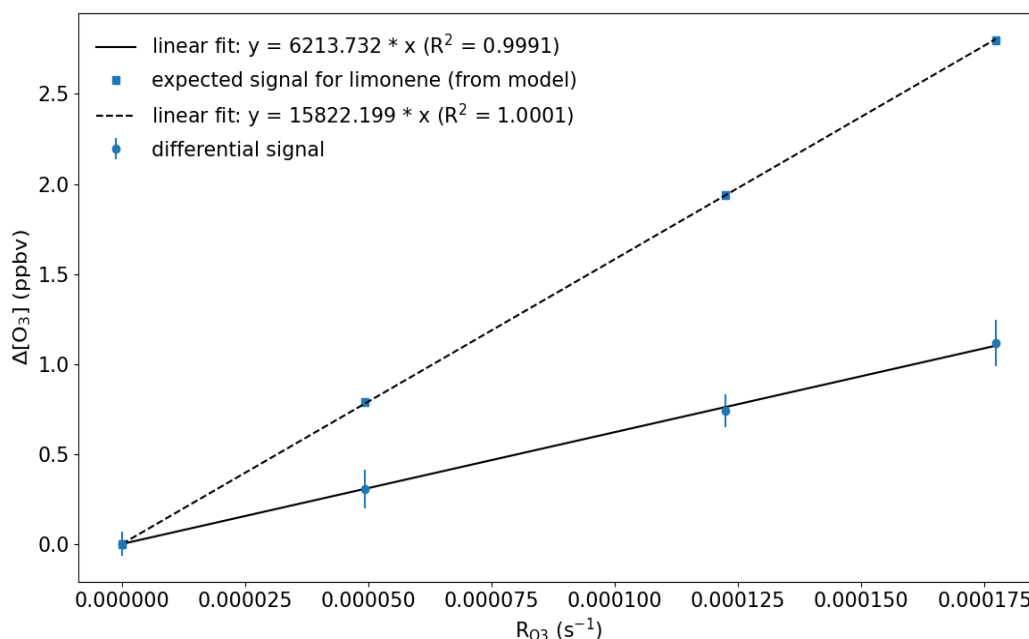


Figure 9

Laboratory test of the TORM. A small flow of a high mole fraction limonene standard was fed into the system upstream of the reactor. The theoretical reactivity calculated from the BVOC ozone rate constant, ozone mole fraction, and residence time are given on the x-axis. Error bars represent the standard deviation for the monitoring data at each level.

537

538 observed during enclosure experiments) and represents upper limit values ~~for the mole fraction~~.
539 The TORM determination shows good linearity, with a R^2 result of the linear regression of 0.9991. At
540 the highest limonene level, the TORM signal, recorded with the differential ozone monitor, was 0.9
541 ppb (after subtraction of the 1.7 ppb $\Delta\Delta$ ozone reactor background that was determined for this
542 particular application).

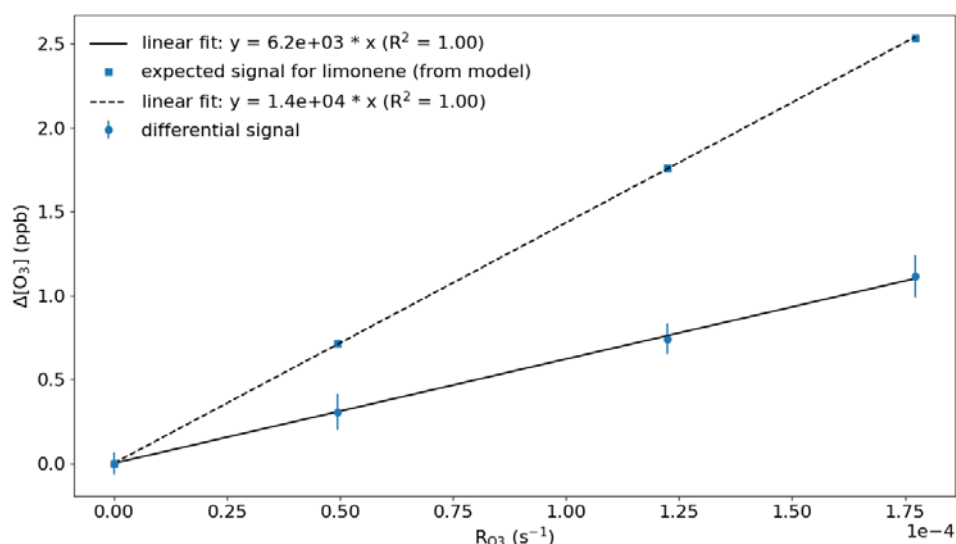


Figure 9. Laboratory test of the TORM. A small flow of a high mole fraction limonene standard was fed into the system upstream of the reactor. The theoretical reactivity calculated from the BVOC ozone rate constant, ozone mole fraction, and residence time are given on the x-axis. Error bars represent the standard deviation for the monitoring data at each level.

543 In Fig. 9, the experimental results from the limonene experiments are also compared with the
 544 ~~modeled~~ modelled signal for various O_3 reactivity values for limonene for the operating conditions of
 545 TORM during this experiment. The ~~modeled~~ modelled results reflect the expected O_3 decrease due
 546 to the reaction with limonene after the reaction corresponding to the ~~theoretical~~ residence time in
 547 the reactor (here ~~167150~~ s; 3.6 l min^{-1} flow through a 10 L reactor), ~~scaled with a factor 0.9~~. The
 548 applied rate constant for the reaction of ozone with limonene at 298 K is $21 \times 10^{-17} \text{ cm}^3 \text{ s}^{-1}$ [Atkinson
 549 and Arey, 2003]. [Atkinson and Arey, 2003]. A linear regression shows that $\Delta[O_3]$ is linearly dependent
 550 with R_{O_3} (~~ca. slope value of $1.5 \text{ ppbv}/(10^{-4} \times 10^4 \text{ ppb s}^{-1})$~~). The discrepancy between the model and
 551 the experiment stem likely from the uncertainty of the mixing ratio in the limonene standard. The
 552 experimentally determined ~~sensitivity response of the differential monitor~~, i.e. ~~approximately 0.5~~
 553 ~~$\text{ppbv}/(10^{-4} \times 6.2 \times 10^3 \text{ ppb s}^{-1})$~~ , is therefore a lower limit. Applying a lower limonene mole fraction in
 554 the standard would lead to a proportionally higher value.

555
 556 The TORM has been deployed in field settings at several research sites in the U.S. and in Finland.
 557 ~~Fig. Figure~~ 10 displays ~~more~~ results from one of these field experiments, i.e. a 3-day branch enclosure
 558 experiment on a red oak tree at the University of Michigan Biological Station. These data show results from
 559 the 2nd and 3rd days of the experiment. The experiment was conducted on relatively warm and sunny days as
 560 can be seen in the radiation and temperature data. Besides the ~~ozone reactivity differential~~ signal, shown in
 561 panel A, the figure also includes the concurrent measurements of ~~respiration and photosynthesis (B)~~,
 562 photochemical active radiation (PAR) (B), ~~respiration and photosynthesis (C)~~, ~~and as well as ambient~~ leaf
 563 and enclosure ~~temperature temperatures~~ (D). The change in humidity, reaching a maximum of on the order
 564 of ~~25 parts per thousand~~‰ as the mid-day maximum when foliage respiration peaks, confirms our estimate
 565 presented in the introduction section for the humidity changes during vegetation enclosure experiments.
 566 Emission samples collected from this enclosure and analyzed by gas-chromatography showed that emissions

567 from this branch were dominated by isoprene, with further substantial emissions of MT and SQT compounds.
568 On both days, the TORM recorded a mid-day maximum differential ozone signal of 12-14 ppb, dropping to 2-
569 3 ppb at night. The instrument readings are quite similar on both days. The ~~ozone reactivity~~differential signal
570 clearly follows a daily cycle, with low values during nighttime hours, and daytime maxima during the early
571 afternoon. The ozone reactivity signal

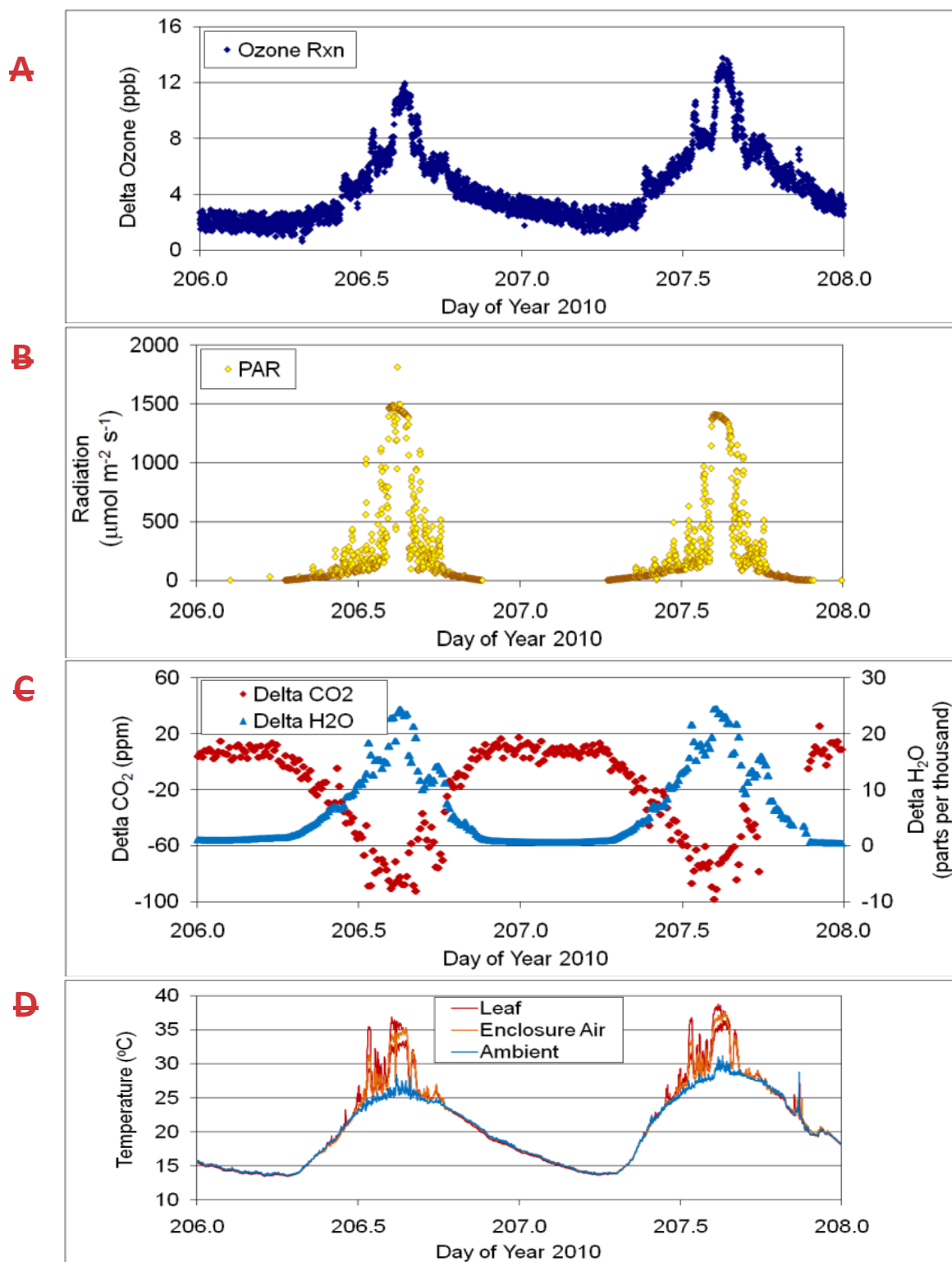
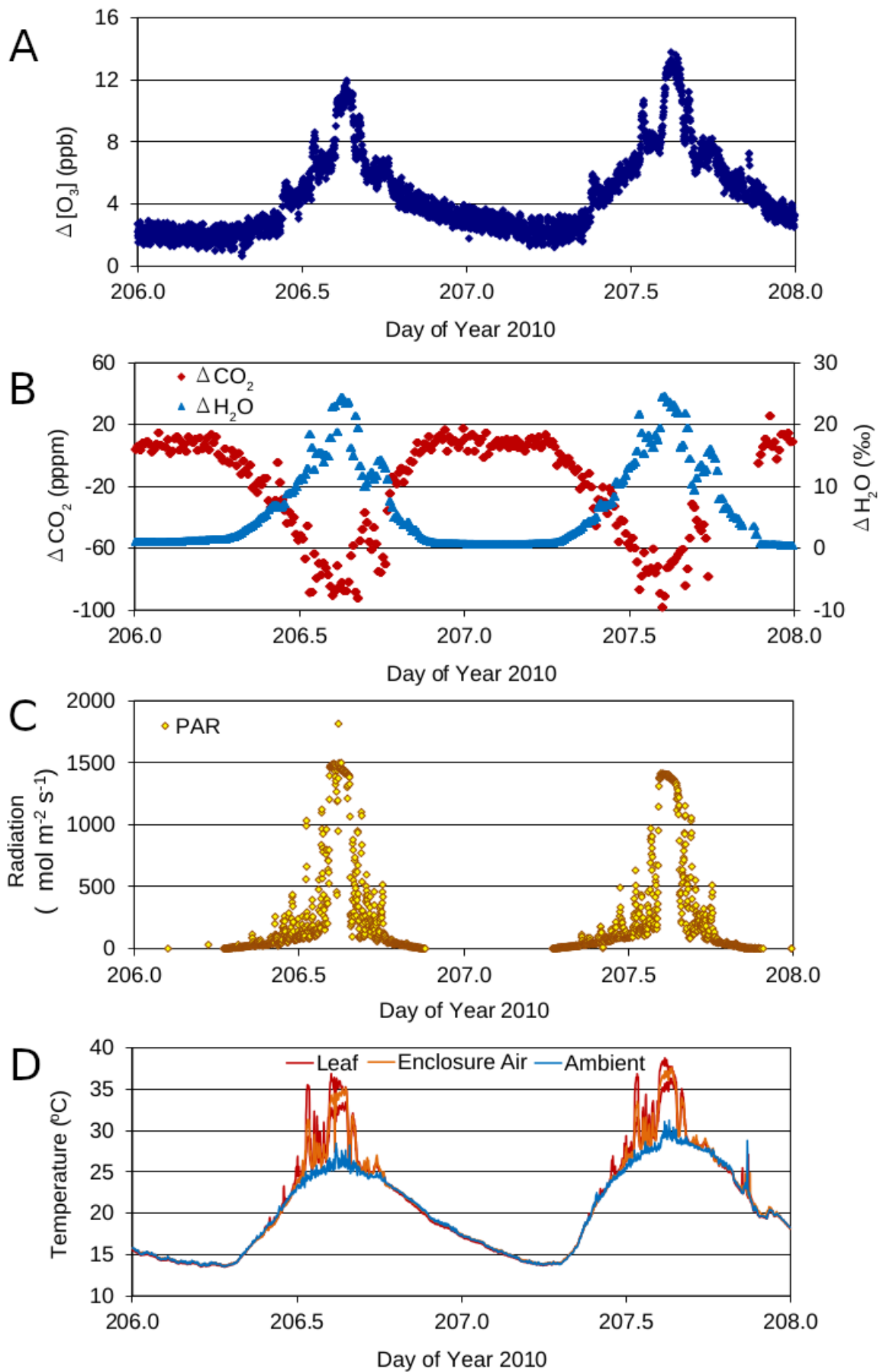


Figure 10

Results obtained over two days from a branch enclosure experiment on a red oak tree, with data for the ozone reactivity measurement (A), solar radiation (B), respiration and photosynthesis expressed as the difference in the water and CO₂ mole fractions in the air stream going into and out of the enclosure (C), and leaf, inside enclosure, and ambient temperature (D).

572
573
574
575

maxima coincide with the peak in diurnal radiation, respiration, and photosynthesis, which suggests that the ozone-reactive emissions are modulated by light availability. Comparison of the observed ozone reactivity with the calculated



576 **Figure 10.** Results obtained over two days from a branch enclosure experiment on a red oak tree, with data
 577 for $\Delta[\text{O}_3]$ measurements (A), solar radiation (B), respiration and photosynthesis expressed as the difference in
 578 the water and CO_2 mole fractions in the air stream going into and out of the enclosure (C), and leaf, inside
 579 enclosure, and ambient temperature (D).

580 ozone reactivity from identified BVOC species could only account for a fraction of the observed
581 reactivity (Praplan et al., manuscript in preparation). Similar diurnal cycles of ozone reactivity were
582 observed for sweetgum in the Southern Oxidant and Aerosol Study [Park et al., 2013], [Park et al.,
583 2013], as can be seen in the ten days of measurements shown in Fig. 5. Please note that the data
584 in Fig. 5 were normalized to the leaf dry mass of the enclosure foliage.
585

586 A presentation of the ozone reactivity results normalized to the leaf dry mass and as a function of
587 leaf temperature for experiments performed at UMBS is shown in Fig. 11. All four species show an
588 increase of reactivity with increasing temperature. This feature indicates that all species emit reactive
589 volatiles at increasing rates as temperature increases. Interestingly, the normalized reactivity for the
590 various tree species is quite different, varying by at least a factor of three. It also appears that the
591 temperature dependencies are different, with red maple showing a more dynamic increase than
592 other species. Remarkably, white pine, a high MT emitter, gave the lowest reactivity results.
593 Furthermore, red maple results appear to be higher than for red oak, despite the fact that red oak
594 was found to emit high amounts of BVOC, totaling ≈ 100 x those of maple, but with most of
595 the emissions made up by isoprene. The relatively high levels of ozone reactivity are also noteworthy
596 in light of the independent OH reactivity study by Kim et al. [2011], Kim et al. [2011], who found that
597 red maple emissions exhibited the highest missing OH reactivity associated with SQT in comparison
598 with these other three species. Consequently, red maple is a prime candidate for having reactive
599 BVOC emissions that hitherto have not been chemically identified.

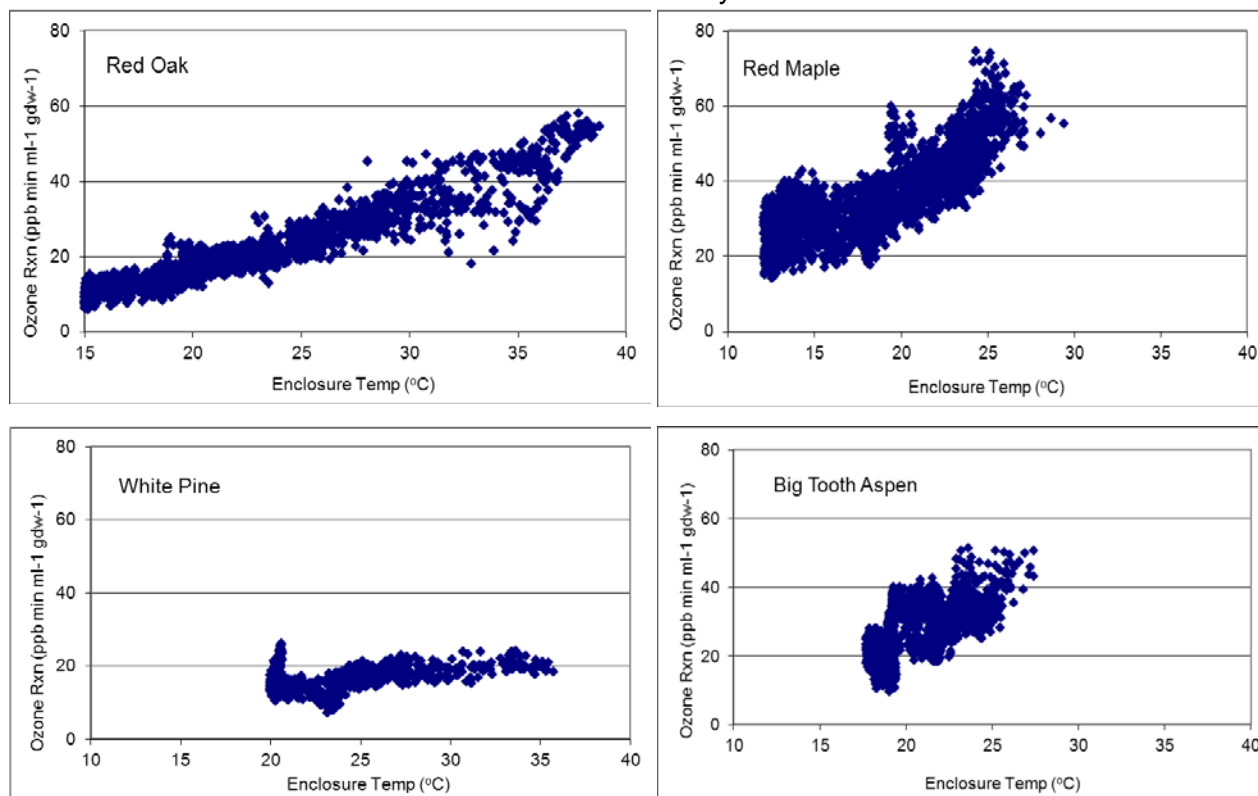


Figure 11

Ozone reactivity results from experiments on red oak, red maple, white pine, and big tooth aspen, normalized to the amount of leaf dry mass and flow rate, as a function of enclosure temperature.

600
601

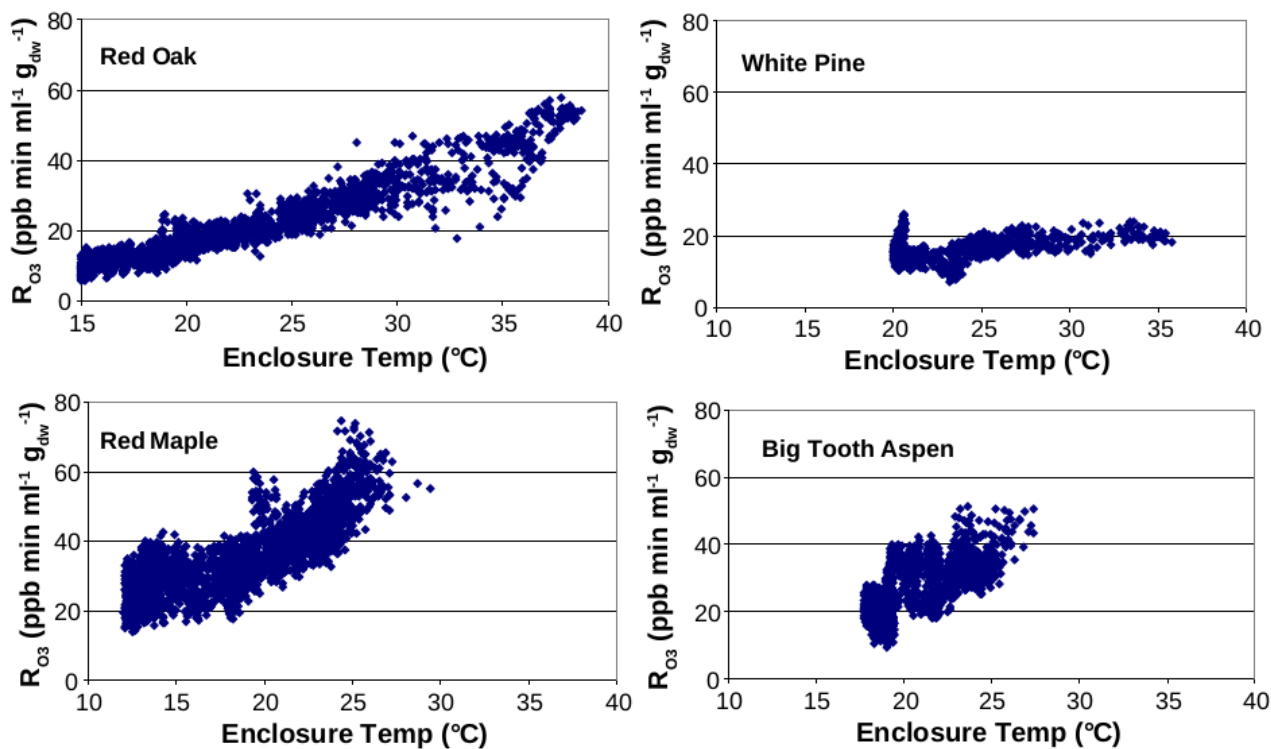


Figure 11. Delta ozone results from experiments on red oak, red maple, white pine, and big tooth aspen, normalized to the amount of leaf dry mass and flow rate, as a function of enclosure temperature.

602

603 4. Summary and Conclusions

604

605 A total ozone reactivity monitor, TORM, was developed for the study of the ozone reactivity of
 606 biogenic emissions. TORM builds on standard laboratory equipment and can be assembled with
 607 moderate technically skilled personnel and at relatively moderate cost. The instrument was
 608 thoroughly characterized, and a number of ameliorations were implemented that significantly
 609 improved the measurement sensitivity and reduced the interference from absolute and changing
 610 water vapor in the sample air. Critical improvements over previously reported measurement
 611 approaches were the adaptation of a commercial ozone UV absorption monitor for direct
 612 measurement of the reacted ozone (ozone differential), heating and temperature control of the
 613 reactor, and the drying of the sample flows with Nafion dryers. Specific challenges arose with this
 614 setup that could be overcome, such as balancing the pressure difference for each cell in the
 615 differential ozone monitor (one cell measuring before the reactor and the other cell measuring after).

616

617 TORM has been used in a number of field settings and proven the feasibility and value of this new
 618 measurement. ~~Ozone reactivity~~Differential ozone signals ($\Delta[O_3]$) on the order of 0-5-9 ppb have been
 619 obtained in enclosure experiments on high-BVOC emitting species. These signals are 20-50 times
 620 above the noise level of the measurement. Chemical identification of BVOC emissions from the
 621 enclosure and estimation of the total reactivity of identified emissions has been able to only account
 622 for a fraction of the directly measured ozone reactivity. Detailed description of these field studies and
 623 discussion of the results, including the attribution of the directly measured ozone reactivity to
 624 identified BVOC emissions, will be presented in a forthcoming publication (Praplan et al., in
 625 preparation).

626

627

628 **Data availability**

629
630 All data that the work builds on are presented in the manuscript and Supplemental Information.

631
632 **Disclaimer**

633
634 This study does not necessarily reflect the views of the funding agencies, and no official
635 endorsements should be inferred.

636
637 **Funding Information**

638
639 The development and testing of the TORM system has been made possible through funding from
640 the U.S. National Science Foundation, grants #AGS 0904139, ATM_-1140571, and AGS-1561755,
641 as well as funding from the Academy of Finland (decisions nos. 307797 and 314099).

642
643
644 **Author contribution**

645
646 D.H. Principal Investigator of the U.S. study, [advised student researchers](#), managed research grants,
647 oversaw the study, prepared and approved the manuscript.

648
649 A.G. Co-Principal Investigator of the U.S. study, reviewed and approved the manuscript.

650
651 J.H. Constructed instrumentation and conducted experiments, developed control and data
652 acquisition software, approved the manuscript.

653
654 R.D. Constructed instrumentation and conducted experiments, participated in field studies, reviewed
655 and approved the manuscript.

656
657 W.W.- Constructed instrumentation, conducted experiments, prepared, reviewed, and approved the
658 manuscript.

659
660 J.H.P. Constructed instrumentation, developed instrument control software, conducted lab and field
661 experiments, reviewed and approved the manuscript.

662
663 A.L. Constructed instrumentation, conducted lab and field experiments, approved the manuscript.

664
665 A.P.P. Principal Investigator of the Finnish study, conducted field and lab experiments, prepared and
666 approved the manuscript.

667
668 **Competing Interests**

669
670 The authors declare that they have no conflict of interest.

671
672 **References**

673 [Altimir, N., P. Kolari, J. P. Tuovinen, T. Vesala, J. Back, T. Suni, M. Kulmala, and P. Hari \(2006\), Foliage surface ozone](#)
674 [deposition: a role for surface moisture?, *Biogeosciences*, 3, 209–228.](#)

675 [Altimir, N., J. P. Tuovinen, T. Vesala, M. Kulmala, and P. Hari \(2004\), Measurements of ozone removal by Scots pine](#)
676 [shoots: calibration of a stomatal uptake model including the non-stomatal component, *Atmospheric Environment*, 38,](#)
677 [2387–2398, doi:10.1016/j.atmosenv.2003.09.077.](#)

678 Atkinson, R., and J. Arey (2003), Gas-phase tropospheric chemistry of biogenic volatile organic compounds: a review,
679 *Atmospheric Environment*, *37*, S197–S219, doi:10.1016/s1352-2310(03)00391-1.

680 Bocquet, F., D. Helmig, B. A. Van Dam, and C. W. Fairall (2011), Evaluation of the flux gradient technique for
681 measurement of ozone surface fluxes over snowpack at Summit, Greenland, *Atmospheric Measurement Techniques*, *4*,
682 2305–2321, doi:10.5194/amt-4-2305-2011.

683 Bouvier-Brown, N. C., A. H. Goldstein, D. R. Worton, D. M. Matross, J. B. Gilman, W. C. Kuster, D. Welsh-Bon, C. Warneke,
684 J. A. de Gouw, T. M. Cahill, and R. Holzinger (2009a), Methyl chavicol: characterization of its biogenic emission rate,
685 abundance, and oxidation products in the atmosphere, *Atmospheric Chemistry and Physics*, *9*, 2061–2074.

686 Bouvier-Brown, N. C., R. Holzinger, K. Palitzsch, and A. H. Goldstein (2009b), Large emissions of sesquiterpenes and
687 methyl chavicol quantified from branch enclosure measurements, *Atmospheric Environment*, *43*, 389–401,
688 doi:10.1016/j.atmosenv.2008.08.039.

689 Boylan, P., D. Helmig, and J. H. Park (2014), Characterization and mitigation of water vapor effects in the measurement
690 of ozone by chemiluminescence with nitric oxide, *Atmospheric Measurement Techniques*, *7*, 1231–1244,
691 doi:10.5194/amt-7-1231-2014.

692 Di Carlo, P., W. H. Brune, M. Martinez, H. Harder, R. Lesher, X. R. Ren, T. Thornberry, M. A. Carroll, V. Young, P. B.
693 Shepson, D. Riemer, E. Apel, and C. Campbell (2004), Missing OH reactivity in a forest: Evidence for unknown reactive
694 biogenic VOCs, *Science*, *304*, 722–725.

695 Duhl, T. R., D. Helmig, and A. Guenther (2008), Sesquiterpene emissions from vegetation: a review, *Biogeosciences*, *5*,
696 761–777.

697 Fares, S., A. Goldstein, and F. Loreto (2010a), Determinants of ozone fluxes and metrics for ozone risk assessment in
698 plants, *Journal of Experimental Botany*, *61*, 629–633, doi:10.1093/jxb/erp336.

699 Fares, S., M. McKay, R. Holzinger, and A. H. Goldstein (2010b), Ozone fluxes in a *Pinus ponderosa* ecosystem are
700 dominated by non-stomatal processes: Evidence from long-term continuous measurements, *Agricultural and Forest
701 Meteorology*, *150*, 420–431.

702 Fares, S., J. H. Park, E. Ormeno, D. R. Gentner, M. McKay, F. Loreto, J. Karlik, and A. H. Goldstein (2010c), Ozone uptake
703 by citrus trees exposed to a range of ozone concentrations, *Atmospheric Environment*, *44*, 3404–3412,
704 doi:10.1016/j.atmosenv.2010.06.010.

705 Goldstein, A. H., M. McKay, M. R. Kurpius, G. W. Schade, A. Lee, R. Holzinger, and R. A. Rasmussen (2004), Forest thinning
706 experiment confirms ozone deposition to forest canopy is dominated by reaction with biogenic VOCs, *Geophysical
707 Research Letters*, *31*, doi:10.1029/2004gl021259.

708 10.1029/2004gl021259.

709 Helmig, D., R. Daly, and S. B. Bertman (2010), Ozone reactivity of biogenic volatile organic compounds from four
710 dominant tree species at PROPHET-CABINEX, *Abstract A53C-0240, 2010 Fall Meeting, AGU, San Francisco, Calif., 13–17
711 Dec.*

712 Hogg, A., J. Uddling, D. Ellsworth, M. A. Carroll, S. Pressley, B. Lamb, and C. Vogel (2007), Stomatal and non-stomatal
713 fluxes of ozone to a northern mixed hardwood forest, *Tellus Series B-Chemical and Physical Meteorology*, *59*, 514–525,
714 doi:10.1111/j.1600-0889.2007.00269.x.

715 Holzinger, R., A. Lee, K. T. Paw, and A. H. Goldstein (2005), Observations of oxidation products above a forest imply
716 biogenic emissions of very reactive compounds, *Atmospheric Chemistry and Physics*, *5*, 67–75.

717 Kim, D. J., T. V. Dinh, J. Y. Lee, I. Y. Choi, D. J. Son, I. Y. Kim, Y. Sunwoo, and J. C. Kim (2019), Effects of Water Removal
718 Devices on Ambient Inorganic Air Pollutant Measurements, *International journal of environmental research and public
719 health*, *16*, 9, doi:10.3390/ijerph16183446.

720 Kim, D. J., T. V. Dinh, J. Y. Lee, D. J. Son, and J. C. Kim (2020), Effect of Nafion Dryer and Cooler on Ambient Air Pollutant
721 (O₃, SO₂, CO) Measurement, *Asian J. Atmos. Environ.*, *14*, 28–34, doi:10.5572/ajae.2020.14.1.028.

722 Kim, S., A. Guenther, T. Karl, and J. Greenberg (2011), Branch-level measurement of total OH reactivity for constraining
723 unknown BVOC emission during CABINEX (Community Atmosphere Biosphere INTERactions Experiments) 09 field
724 campaign, *Atmos. Chem. Phys. Discuss.*, *11*, 7781–7809.

725 Kurpius, M. R., and A. H. Goldstein (2003), Gas-phase chemistry dominates O₃ loss to a forest, implying a source of
726 aerosols and hydroxyl radicals to the atmosphere, *Geophysical Research Letters*, *30*, doi:10.1029/2002gl016785.

727 10.1029/2002gl016785.

728 [Lenschow, D. H., R. Pearson, and B. B. Stankov \(1981\), Estimating the ozone budget in the boundary layer by use of](#)
729 [aircraft measurements of ozone eddy flux and mean concentration, *Journal of Geophysical Research-Oceans*, *86*, 7291-](#)
730 [7297, doi:10.1029/JC086iC08p07291.](#)

731 [Lenschow, D. H., R. Pearson, and B. B. Stankov \(1982\), Measurements of ozone vertical flux to ocean and forest, *Journal*](#)
732 [of *Geophysical Research-Oceans and Atmospheres*, *87*, 8833-8837, doi:10.1029/JC087iC11p08833.](#)

733 [Lou, S., F. Holland, F. Rohrer, K. Lu, B. Bohn, T. Brauers, C. C. Chang, H. Fuchs, R. Haseler, K. Kita, Y. Kondo, X. Li, M. Shao,](#)
734 [L. Zeng, A. Wahner, Y. Zhang, W. Wang, and A. Hofzumahaus \(2010\), Atmospheric OH reactivities in the Pearl River Delta](#)
735 [—China in summer 2006: measurement and model results, *Atmospheric Chemistry and Physics*, *10*, 11243-11260,](#)
736 [doi:10.5194/acp-10-11243-2010.](#)

737 [Matsumoto, J. \(2014\), Measuring Biogenic Volatile Organic Compounds \(BVOCs\) from Vegetation in Terms of Ozone](#)
738 [Reactivity, *Aerosol Air Qual. Res.*, *14*, 197-206, doi:10.4209/aaqr.2012.10.0275.](#)

739 [Matthews, R. D., R. F. Sawyer, and R. W. Schefer \(1977\), Interferences in chemiluminescence measurement of NO and](#)
740 [NO₂ emissions from combustion systems, *Environ. Sci. Technol.*, *11*, 1092-1096.](#)

741 [McKinney, K. A., B. H. Lee, A. Vasta, T. V. Pho, and J. W. Munger \(2011\), Emissions of isoprenoids and oxygenated](#)
742 [biogenic volatile organic compounds from a New England mixed forest, *Atmos. Chem. Phys.*, *11*, 4807-4831.](#)

743 [Misztal, P. K., S. M. Owen, A. B. Guenther, R. Rasmussen, C. Geron, P. Harley, G. J. Phillips, A. Ryan, D. P. Edwards, C. N.](#)
744 [Hewitt, E. Nemitz, J. Siong, M. R. Heal, and J. N. Cape \(2010\), Large estragole fluxes from oil palms in Borneo,](#)
745 [Atmospheric Chemistry and Physics, *10*, 4343-4358, doi:10.5194/acp-10-4343-2010.](#)

746 [Ortega, J., and D. Helmig \(2008\), Approaches for quantifying reactive and low volatility biogenic organic compound](#)
747 [emissions by vegetation enclosure techniques — Part A, *Chemosphere*, *72*, 343-364,](#)
748 [doi:10.1016/j.chemosphere.2007.11.020.](#)

749 [Ortega, J., D. Helmig, R. W. Daly, D. M. Tanner, A. B. Guenther, and J. D. Herrick \(2008\), Approaches for quantifying](#)
750 [reactive and low volatility biogenic organic compound emissions by vegetation enclosure techniques — Part B:](#)
751 [Applications, *Chemosphere*, *72*, 365-380, doi:10.1016/j.chemosphere.2008.02.054.](#)

752 [Ortega, J., D. Helmig, A. Guenther, P. Harley, S. Pressley, and C. Vogel \(2007\), Flux estimates and OH reaction potential](#)
753 [of reactive biogenic volatile organic compounds \(BVOCs\) from a mixed northern hardwood forest, *Atmospheric*](#)
754 [Environment, *41*, 5479-5495, doi:10.1016/j.atmosenv.2006.12.033.](#)

755 [Park, J., A. B. Guenther, and D. Helmig \(2013\), Ozone reactivity of biogenic volatile organic compound \(BVOC\) emissions](#)
756 [during the Southeast Oxidant and Aerosol Study \(SOAS\), in *American Geophysical Union, Fall Meeting 2013, abstract*](#)
757 [#A13A-0172, edited.](#)

758 [Ridley, B. A., F. E. Grahek, and J. G. Walega \(1992\), A small, high sensitivity, medium response ozone detector suitable](#)
759 [for measurements from light aircraft, *Journal of Atmospheric and Oceanic Technology*, *9*, 142-148, doi:10.1175/1520-](#)
760 [0426\(1992\)009<0142:ashsmr>2.0.co;2-](#)

761 [Sommariva, R., L. J. Kramer, L. R. Crilley, M. S. Alam, and W. J. Bloss \(2020\), An instrument for in situ measurement of](#)
762 [total ozone reactivity, *Atmospheric Measurement Techniques*, *13*, 1655-1670, doi:10.5194/amt-13-1655-2020.](#)

763 [Spicer, C. W., D. W. Joseph, and W. M. Ollison \(2010\), A Re-Examination of Ambient Air Ozone Monitor Interferences,](#)
764 [Journal of the Air & Waste Management Association, *60*, 1353-1364, doi:10.3155/1047-3289.60.11.1353.](#)

765 [Wilson, K. L., and J. W. Birks \(2006\), Mechanism and elimination of a water vapor interference in the measurement of](#)
766 [ozone by UV absorbance, *Environmental Science & Technology*, *40*, 6361-6367, doi:10.1021/es052590c.](#)

767 [Wolfe, G. M., J. A. Thornton, W. A. McKay, and A. H. Goldstein \(2011\), Forest-atmosphere exchange of ozone: Sensitivity](#)
768 [to very reactive biogenic VOC emissions and implications for in-canopy photochemistry, *Atmos. Chem. Phys. Discuss.*,](#)
769 [11, 13381-13424.](#)

770 [Altimir, N., P. Kolari, J. P. Tuovinen, T. Vesala, J. Back, T. Suni, M. Kulmala, and P. Hari \(2006\), Foliage surface](#)
771 [ozone deposition: a role for surface moisture?, *Biogeosciences*, *3*, 209-228.](#)

772 [Altimir, N., J. P. Tuovinen, T. Vesala, M. Kulmala, and P. Hari \(2004\), Measurements of ozone removal by Scots](#)
773 [pine shoots: calibration of a stomatal uptake model including the non-stomatal component, *Atmospheric*](#)
774 [Environment, *38*, 2387-2398, doi:10.1016/j.atmosenv.2003.09.077.](#)

775 [Atkinson, R., and J. Arey \(2003\), Gas-phase tropospheric chemistry of biogenic volatile organic compounds: a](#)
776 [review, *Atmospheric Environment*, *37*, S197-S219, doi:10.1016/s1352-2310\(03\)00391-1.](#)

777 [Bocquet, F., D. Helmig, B. A. Van Dam, and C. W. Fairall \(2011\), Evaluation of the flux gradient technique for](#)
778 [measurement of ozone surface fluxes over snowpack at Summit, Greenland, Atmospheric Measurement](#)
779 [Techniques, 4, 2305-2321, doi:10.5194/amt-4-2305-2011.](#)

780 [Bouvier-Brown, N. C., A. H. Goldstein, D. R. Worton, D. M. Matross, J. B. Gilman, W. C. Kuster, D. Welsh-Bon,](#)
781 [C. Warneke, J. A. de Gouw, T. M. Cahill, and R. Holzinger \(2009a\), Methyl chavicol: characterization of its](#)
782 [biogenic emission rate, abundance, and oxidation products in the atmosphere, Atmospheric Chemistry and](#)
783 [Physics, 9, 2061-2074.](#)

784 [Bouvier-Brown, N. C., R. Holzinger, K. Palitzsch, and A. H. Goldstein \(2009b\), Large emissions of sesquiterpenes](#)
785 [and methyl chavicol quantified from branch enclosure measurements, Atmospheric Environment, 43, 389-](#)
786 [401, doi:10.1016/j.atmosenv.2008.08.039.](#)

787 [Boylan, P., D. Helmig, and J. H. Park \(2014\), Characterization and mitigation of water vapor effects in the](#)
788 [measurement of ozone by chemiluminescence with nitric oxide, Atmospheric Measurement Techniques, 7,](#)
789 [1231-1244, doi:10.5194/amt-7-1231-2014.](#)

790 [Damian, V., Sandu, A., Damian, M., Potra, F., and Carmichael, G. \(2002\), The kinetic preprocessor KPP—A](#)
791 [software environment for solving chemical kinetics, Computers & Chemical Engineering, 26, 1567–1579.](#)
792 [doi:10.1016/S0098-1354\(02\)00128-X.](#)

793 [Di Carlo, P., W. H. Brune, M. Martinez, H. Harder, R. Leshner, X. R. Ren, T. Thornberry, M. A. Carroll, V. Young, P.](#)
794 [B. Shepson, D. Riemer, E. Apel, and C. Campbell \(2004\), Missing OH reactivity in a forest: Evidence for](#)
795 [unknown reactive biogenic VOCs, Science, 304, 722-725.](#)

796 [Duhl, T. R., D. Helmig, and A. Guenther \(2008\), Sesquiterpene emissions from vegetation: a review,](#)
797 [Biogeosciences, 5, 761-777.](#)

798 [Fares, S., A. Goldstein, and F. Loreto \(2010a\), Determinants of ozone fluxes and metrics for ozone risk](#)
799 [assessment in plants, Journal of Experimental Botany, 61, 629-633, doi:10.1093/jxb/erp336.](#)

800 [Fares, S., M. McKay, R. Holzinger, and A. H. Goldstein \(2010b\), Ozone fluxes in a Pinus ponderosa ecosystem](#)
801 [are dominated by non-stomatal processes: Evidence from long-term continuous measurements, Agricultural](#)
802 [and Forest Meteorology, 150, 420-431.](#)

803 [Fares, S., J. H. Park, E. Ormeno, D. R. Gentner, M. McKay, F. Loreto, J. Karlik, and A. H. Goldstein \(2010c\), Ozone](#)
804 [uptake by citrus trees exposed to a range of ozone concentrations, Atmospheric Environment, 44, 3404-3412,](#)
805 [doi:10.1016/j.atmosenv.2010.06.010.](#)

806 [Goldstein, A. H., M. McKay, M. R. Kurpius, G. W. Schade, A. Lee, R. Holzinger, and R. A. Rasmussen \(2004\),](#)
807 [Forest thinning experiment confirms ozone deposition to forest canopy is dominated by reaction with](#)
808 [biogenic VOCs, Geophysical Research Letters, 31, doi:L22106](#)
809 [10.1029/2004gl021259.](#)

810 [Helmig, D., R. Daly, and S. B. Bertman \(2010\), Ozone reactivity of biogenic volatile organic compounds from](#)
811 [four dominant tree species at PROPHET-CABINEX, Abstract A53C-0240, 2010 Fall Meeting, AGU, San](#)
812 [Francisco, Calif., 13-17 Dec. .](#)

813 [Hogg, A., J. Uddling, D. Ellsworth, M. A. Carroll, S. Pressley, B. Lamb, and C. Vogel \(2007\), Stomatal and non-](#)
814 [stomatal fluxes of ozone to a northern mixed hardwood forest, Tellus Series B-Chemical and Physical](#)
815 [Meteorology, 59, 514-525, doi:10.1111/j.1600-0889.2007.00269.x.](#)

816 [Holzinger, R., A. Lee, K. T. Paw, and A. H. Goldstein \(2005\), Observations of oxidation products above a forest](#)
817 [imply biogenic emissions of very reactive compounds, Atmospheric Chemistry and Physics, 5, 67-75.](#)

818 [Kim, D. J., T. V. Dinh, J. Y. Lee, I. Y. Choi, D. J. Son, I. Y. Kim, Y. Sunwoo, and J. C. Kim \(2019\), Effects of Water](#)
819 [Removal Devices on Ambient Inorganic Air Pollutant Measurements, International journal of environmental](#)
820 [research and public health, 16, 9, doi:10.3390/ijerph16183446.](#)

821 [Kim, D. J., T. V. Dinh, J. Y. Lee, D. J. Son, and J. C. Kim \(2020\), Effect of Nafion Dryer and Cooler on Ambient Air](#)
822 [Pollutant \(O₃, SO₂, CO\) Measurement, Asian J. Atmos. Environ., 14, 28-34, doi:10.5572/ajae.2020.14.1.028.](#)

823 [Kim, S., A. Guenther, T. Karl, and J. Greenberg \(2011\), Branch-level measurement of total OH reactivity for](#)
824 [constraining unknown BVOC emission during CABINEX \(Community Atmosphere-Biosphere INteractions](#)
825 [Experiments\)-09 field campaign, Atmos. Chem. Phys. Discuss., 11, 7781-7809.](#)

826 [Kurpius, M. R., and A. H. Goldstein \(2003\), Gas-phase chemistry dominates O-3 loss to a forest, implying a](#)
827 [source of aerosols and hydroxyl radicals to the atmosphere, Geophysical Research Letters, 30,](#)
828 [doi:10.1029/2002gl016785.](#)

829 [Lenschow, D. H., R. Pearson, and B. B. Stankov \(1981\), Estimating the ozone budget in the boundary-layer by](#)
830 [use of aircraft measurements of ozone flux and mean concentration, Journal of Geophysical Research-](#)
831 [Oceans, 86, 7291-7297, doi:10.1029/JC086iC08p07291.](#)

832 [Lenschow, D. H., R. Pearson, and B. B. Stankov \(1982\), Measurements of ozone vertical flux to ocean and](#)
833 [forest, Journal of Geophysical Research-Oceans and Atmospheres, 87, 8833-8837,](#)
834 [doi:10.1029/JC087iC11p08833.](#)

835 [Lou, S., F. Holland, F. Rohrer, K. Lu, B. Bohn, T. Brauers, C. C. Chang, H. Fuchs, R. Haseler, K. Kita, Y. Kondo, X.](#)
836 [Li, M. Shao, L. Zeng, A. Wahner, Y. Zhang, W. Wang, and A. Hofzumahaus \(2010\), Atmospheric OH reactivities](#)
837 [in the Pearl River Delta - China in summer 2006: measurement and model results, Atmospheric Chemistry](#)
838 [and Physics, 10, 11243-11260, doi:10.5194/acp-10-11243-2010.](#)

839 [Matsumoto, J. \(2014\), Measuring Biogenic Volatile Organic Compounds \(BVOCs\) from Vegetation in Terms of](#)
840 [Ozone Reactivity, Aerosol Air Qual. Res., 14, 197-206, doi:10.4209/aaqr.2012.10.0275.](#)

841 [Matthews, R. D., R. F. Sawyer, and R. W. Schefer \(1977\), Interferences in chemiluminescence measurement of](#)
842 [NO and NO2 emissions from combustion systems, Environ. Sci. Technol., 11, 1092-1096.](#)

843 [McKinney, K. A., B. H. Lee, A. Vasta, T. V. Pho, and J. W. Munger \(2011\), Emissions of isoprenoids and](#)
844 [oxygenated biogenic volatile organic compounds from a New England mixed forest, Atmos. Chem. Phys., 11,](#)
845 [4807-4831.](#)

846 [Misztal, P. K., S. M. Owen, A. B. Guenther, R. Rasmussen, C. Geron, P. Harley, G. J. Phillips, A. Ryan, D. P.](#)
847 [Edwards, C. N. Hewitt, E. Nemitz, J. Siong, M. R. Heal, and J. N. Cape \(2010\), Large estragole fluxes from oil](#)
848 [palms in Borneo, Atmospheric Chemistry and Physics, 10, 4343-4358, doi:10.5194/acp-10-4343-2010.](#)

849 [Ortega, J., and D. Helmig \(2008\), Approaches for quantifying reactive and low-volatility biogenic organic](#)
850 [compound emissions by vegetation enclosure techniques - Part A, Chemosphere, 72, 343-364,](#)
851 [doi:10.1016/j.chemosphere.2007.11.020.](#)

852 [Ortega, J., D. Helmig, R. W. Daly, D. M. Tanner, A. B. Guenther, and J. D. Herrick \(2008\), Approaches for](#)
853 [quantifying reactive and low-volatility biogenic organic compound emissions by vegetation enclosure](#)
854 [techniques - Part B: Applications, Chemosphere, 72, 365-380, doi:10.1016/j.chemosphere.2008.02.054.](#)

855 [Ortega, J., D. Helmig, A. Guenther, P. Harley, S. Pressley, and C. Vogel \(2007\), Flux estimates and OH reaction](#)
856 [potential of reactive biogenic volatile organic compounds \(BVOCs\) from a mixed northern hardwood forest,](#)
857 [Atmospheric Environment, 41, 5479-5495, doi:10.1016/j.atmosenv.2006.12.033.](#)

858 [Park, J., A. B. Guenther, and D. Helmig \(2013\), Ozone reactivity of biogenic volatile organic compound \(BVOC\)](#)
859 [emissions during the Southeast Oxidant and Aerosol Study \(SOAS\), in American Geophysical Union, Fall](#)
860 [Meeting 2013, abstract #A13A-0172, edited.](#)

861 [Ridley, B. A., F. E. Grahek, and J. G. Walega \(1992\), A small, high-sensitivity, medium-response ozone detector](#)
862 [suitable for measurements from light aircraft, Journal of Atmospheric and Oceanic Technology, 9, 142-148,](#)
863 [doi:10.1175/1520-0426\(1992\)009<0142:ashsmr>2.0.co;2.](#)

864 [Sommariva, R., L. J. Kramer, L. R. Crilley, M. S. Alam, and W. J. Bloss \(2020\), An instrument for in situ](#)
865 [measurement of total ozone reactivity, Atmospheric Measurement Techniques, 13, 1655-1670,](#)
866 [doi:10.5194/amt-13-1655-2020.](#)

867 [Spicer, C. W., D. W. Joseph, and W. M. Ollison \(2010\), A Re-Examination of Ambient Air Ozone Monitor](#)
868 [Interferences, Journal of the Air & Waste Management Association, 60, 1353-1364, doi:10.3155/1047-](#)
869 [3289.60.11.1353.](#)

870 [Wilson, K. L., and J. W. Birks \(2006\), Mechanism and elimination of a water vapor interference in the](#)
871 [measurement of ozone by UV absorbance, Environmental Science & Technology, 40, 6361-6367,](#)
872 [doi:10.1021/es052590c.](#)

873 [Wolfe, G. M., J. A. Thornton, W. A. McKay, and A. H. Goldstein \(2011\), Forest-atmosphere exchange of ozone:](#)
874 [Sensitivity to very reactive biogenic VOC emissions and implications for in-canopy photochemistry, Atmos.](#)
875 [Chem. Phys. Discuss., 11, 13381-13424.](#)